Ecological Modelling 510 (2025) 111282

Contents lists available at ScienceDirect

Ecological Modelling

journal homepage: www.elsevier.com/locate/ecolmodel

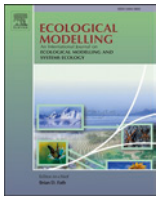

Empirical and mechanistic models predict pinyon ips (*Ips confusus*) phenology

E.M. Hansen [a], J.A. Powell [b], A. Graves [c], S. Souder [c], J.C. Vandygriff [a], M. Gaylord [d], J. McMillin [d], B.J. Bentz [a,*]

[a] USDA Forest Service, Rocky Mountain Research Station, Logan, UT, USA
[b] Department of Mathematics and Statistics, Utah State University, Logan, UT, USA
[c] USDA Forest Service, Forest Health Protection, Albuquerque, NM, USA
[d] USDA forest Service, Forest Health Protection, Flagstaff, AZ, USA

ARTICLE INFO

Keywords:
Process-based model
Empirical model
Phenology
Ips confusus
Temperature-dependent development
Drought

ABSTRACT

Pinyon ips (*Ips confusus* LeConte) is a native bark beetle that can cause extensive mortality of pinyon pines (*Pinus* spp.) in the western United States, particularly during hot droughts that stress trees. Although pinyon ips is assumed to be multivoltine, with multiple generations per year, research is lacking regarding temperature-dependent phenology and field-based evidence of annual generations. At sites in Arizona and New Mexico, across two years, we monitored pinyon ips lifecycle timing using emergence cages on trees and passive traps. These data and associated field-based temperatures were used to develop empirical models that predict timing of spring emergence and summer generations. For comparison to field-based models, laboratory experiments were conducted to quantify pinyon ips lifestage-specific development at constant temperatures and a cohort-based mechanistic phenology model was developed. Field measures highlight extensive overlap of summer generations, likely due to extended oviposition, variable microhabitat temperatures, and developmental variability among lifestages. Predictions from the two models were in alignment with each other and with field-based data for spring emergence of an overwinter generation, and the first and second summer generations. Both models also predicted the observed number of summer generations, although cohort splitting overwinter was difficult to quantify. The warmest sites were predicted to have up to 5 annual generations with 2 generations at cool sites. Increasing severity of hot droughts will likely increase pinyon ips caused tree mortality as the number of annual generations increases. The models can be used to estimate pinyon ips generations given daily temperature records.

1. Introduction

Colorado (*Pinus edulis* Engelm.) and singleleaf pinyon pines (*P. monophylla* Torr. & Frém) are major components of woodland ecosystems in the southwestern US. These woodlands are ecologically, economically, and culturally important and cover about 20 million hectares of Arizona, Nevada, Utah, Colorado, and New Mexico. Common associates include several juniper species, especially Utah juniper (*Juniperus osteopserma* (Torr.) Little) and one-seed juniper (*J. monosperma* (Engelm.) Sarg.) (Barger and Ffolliott, 1972). Pinyon-juniper woodlands represent important ecosystems for rare plants, birds, and other species (Webb, 1999). Pinyon pines are important as fuelwood and fenceposts in rural areas, and the large seeds are a traditional dietary staple for Indigenous cultures, among other services (Harlow et al., 1981).

Pinyon pines are susceptible to sporadic outbreaks of the native bark beetle pinyon ips (*Ips confusus* LeConte Coleoptera: Curculionidae, Scolytinae), especially when the trees are stressed by drought (Gaylord et al., 2013, 2015) or dwarf mistletoe infestation (Negrón and Wilson, 2003). For example, a region-wide drought in the early 2000s was associated with pinyon ips-caused mortality on over 1.2 million hectares in the southwestern US (Kleinman et al., 2012). Pinyon pine mortality approached 100 % in localized areas and, in Arizona, cumulative mortality from 2002–2004 exceeded 20 % of basal area (Shaw et al., 2005). Hot droughts are known to positively influence bark beetle populations (Kolb et al., 2016; Bentz et al., 2023; Potterf et al., 2025), and this

* Corresponding author at: USDA Forest Service, Rocky Mountain Research Station, 860 North 1200 East, Logan, UT 84321, USA.
E-mail address: barbara.bentz@usda.gov (B.J. Bentz).

https://doi.org/10.1016/j.ecolmodel.2025.111282
Received 21 April 2025; Received in revised form 22 July 2025; Accepted 31 July 2025
Available online 8 August 2025
0304-3800/Published by Elsevier B.V.

pinyon ips population eruption ended coincident with the moderation of drought and high temperature conditions (Raffa et al., 2008). Pinyon ips-caused tree mortality is mapped almost yearly during aerial detection surveys (USDA Forest Service, 2025), however, suggesting presence of low level, endemic populations even during non-drought years. Observational studies suggest that patterns of pinyon pine mortality may also be related to stand (tree size, density) and site factors (elevation, topography) but there are also inconsistencies in interpretation (Ogle et al., 2000; Negrón and Wilson, 2003; Greenwood and Weisberg, 2008; Floyd et al., 2009; Santos and Whitham, 2010; Kleinman et al., 2012; Meddens et al., 2015).

Pinyon ips has a distribution roughly coincident with *P. edulis* and *P. monophylla* and outbreaks are less common in other pinyon pine species (Wood, 1982). A polygamous species, males initiate attacks on novel hosts, mining into the phloem of boles and large branches. Males release aggregation pheromones to attract females and conspecifics to overwhelm host defenses. These pheromones have been identified as (+) *ipsdienol, cis*-verbenol, and *ipsenol* (Birch et al., 1977; Seybold et al., 2004). Two to four females mate with each male, then construct separate egg galleries radiating from the central nuptial chamber (Cibrián-Tovar et al., 1995). Following eclosion, larvae feed perpendicular to the egg gallery, consuming phloem which results in host death if attack concentration reaches some threshold level. Following pupation and adult eclosion, brood adults emerge from their natal hosts, completing the life cycle.

Despite the significance of pinyon ips to woodland ecosystems, this organism's phenology, including number of generations per year, is only loosely known, and the impacts of weather variations and climate change are unknown. In a study describing the overwintering life-stages of pinyon ips, Chansler (1964) stated the species has "usually three and sometimes four generations" between April and October but without citation or supporting data. Eager (1999) stated two to five generations per year as a function of elevation and climate but also without citation or supporting data.

Phenology models are important tools for predicting thermally-dependent rates of change in insect population dynamics and can be developed empirically or using a process-based, mechanistic understanding. Empirical models are often based on thermal sums or degree days that are associated with trends in lifestage completion at a given sample of observed locations (Tran et al., 2020; Bentz et al., 2023). In contrast, mechanistic phenology models are based on data describing physiological responses to temperature or other environmental data and can capture nonlinear development across a range of conditions (Powell and Bentz, 2009; Candau and Studens, 2025). Although process-based models can better include novel or no-analog responses that may occur in the future as climate changes, both model types are valuable tools for understanding current lifecycle patterns. Given that empirical models describe responses to specific conditions, rather than physiological responses to a range of conditions, extrapolation of results beyond the area of development is often not warranted. Data for empirical model development, however, are often more easily obtained than for mechanistic model development.

Our goals were to describe pinyon ips life cycle timing from field observations at several sites in New Mexico and Arizona, estimate life stage-specific (egg through pupa) developmental rates and phenology from constant temperature laboratory data, and parameterize empirical and mechanistic models that predict the number of generations per year as a function of temperature. Two empirical sub-models were developed using temperature-based variables best related to field-observed adult emergence, one for emergence of the overwintering generation and one for emergence of summer generations. These two models were combined to estimate number of annual generations. We also developed a mechanistic phenology model based on constant temperature laboratory data of egg, larval and pupal development, augmented with estimates of oviposition and adult development rates. The mechanistic model is a hybrid in that it uses predictions from the overwintering generation empirical sub-model for initiation. Predictions from the two model types are compared to field observations and we apply the models to cool and warm pinyon pine sites to estimate potential changes in numbers of generations with climate change.

2. Materials and methods

2.1. Phenology data – field sites

Field sites were chosen based on abundant currently infested pinyon pines and ease of access to facilitate frequent site visits. Red Mountain, Arizona (35.545 N, 111.859 W, elevation 2046 m) was established 22 March 2022 and Lobo Canyon, New Mexico (35.250 N, 107.705 W, elevation 2514 m) was established 24 March 2022 (Fig. 1). At each site we identified 6–7 *P edulis* infested the previous fall which had overwintering brood adults, henceforth the overwinter generation. When possible, emergence cages were attached on north and south bole aspects of the infested trees using 30 × 60 cm flexible screens centered at breast height (1.4 m) (see Bentz et al., 2023). Due to variation in tree size, attack density, and branch locations, some trees had: 1) cages installed on east or west bole aspects; 2) a single cage; 3) cages installed starting near the root collar; or 4) cages narrower than 30 cm. The bottom of the screen was shaped into a funnel with a transparent centrifuge tube tied on to allow collection of emerging adults.

At each site, near currently infested trees, we deployed six passive traps made with two interlocking polycarbonate sheets (41 × 81 cm), forming an X-pattern when viewed from above. These are intended to intercept flying beetles and are considered to be an unbiased sample of beetle flight activity as opposed to synthetic pheromone-baited funnel traps which can capture bark beetles in patterns out of proportion to overall population trends (Bentz, 2006). A large funnel (~1 m diameter) was attached below the panels to collect falling beetles, and the device was suspended off the ground 1–2 m. A small strip of 2,2-dichlorovinyl dimethyl phosphate-impregnated plastic was added to collection cups to prevent escape and predation.

Additionally, we selected four live pinyon pines, 23–43 cm dbh, central to clumps of currently infested trees. These were baited with a pheromone blend lure consisting of: (+) ipsdienol, *cis*-verbenol, and ipsenol (Synergy Semiochemical Corp., Delta, B.C.) in an attempt to ensure attacks from overwintering brood adults.

Each site was visited twice weekly to collect beetles in the emergence cages and passive traps and to examine baited trees for evidence of attacks (e.g., boring dust and entrance holes). Lures were removed after attacks began and, after about two weeks, emergence cages were attached to bole faces as described above. After baited trees were attacked, the collection interval became weekly but was occasionally skipped because of scheduling conflicts. Collections were brought to the laboratory for sorting, identification, and counting. For the Lobo Canyon site, we identified and counted other coleopterans captured in the cages and traps (Table S2). As cages on the baited trees began to collect emerging brood adults (henceforth the first summer generation), nearby uninfested pinyon pines were examined for evidence of attack. Newly attacked trees were flagged and, after allowing about two weeks for attacks to reach culmination, emergence cages were attached to these trees. This process continued through the end of the warm season, i.e., late October to monitor subsequent summer generations.

At the Lobo Canyon site, the four baited trees were first attacked from day-of-year (DOY) 108–116, yet emergence of overwinter beetles continued through at least DOY 130. For this generation and site-year only, we caged five additional trees with date of first attacks observed from DOY 125–132.

We installed two new sites during 2023. Tusayan, Arizona (35.859 N, 112.146 W, elevation 1935 m) was established 28 March 2023 and Cedro Peak, New Mexico (35.045 N, 106.359 W, elevation 2220 m) was established 29–30 March 2023 (Fig. 1). Each site had four *P. edulis* identified as having overwintering brood adults and we deployed

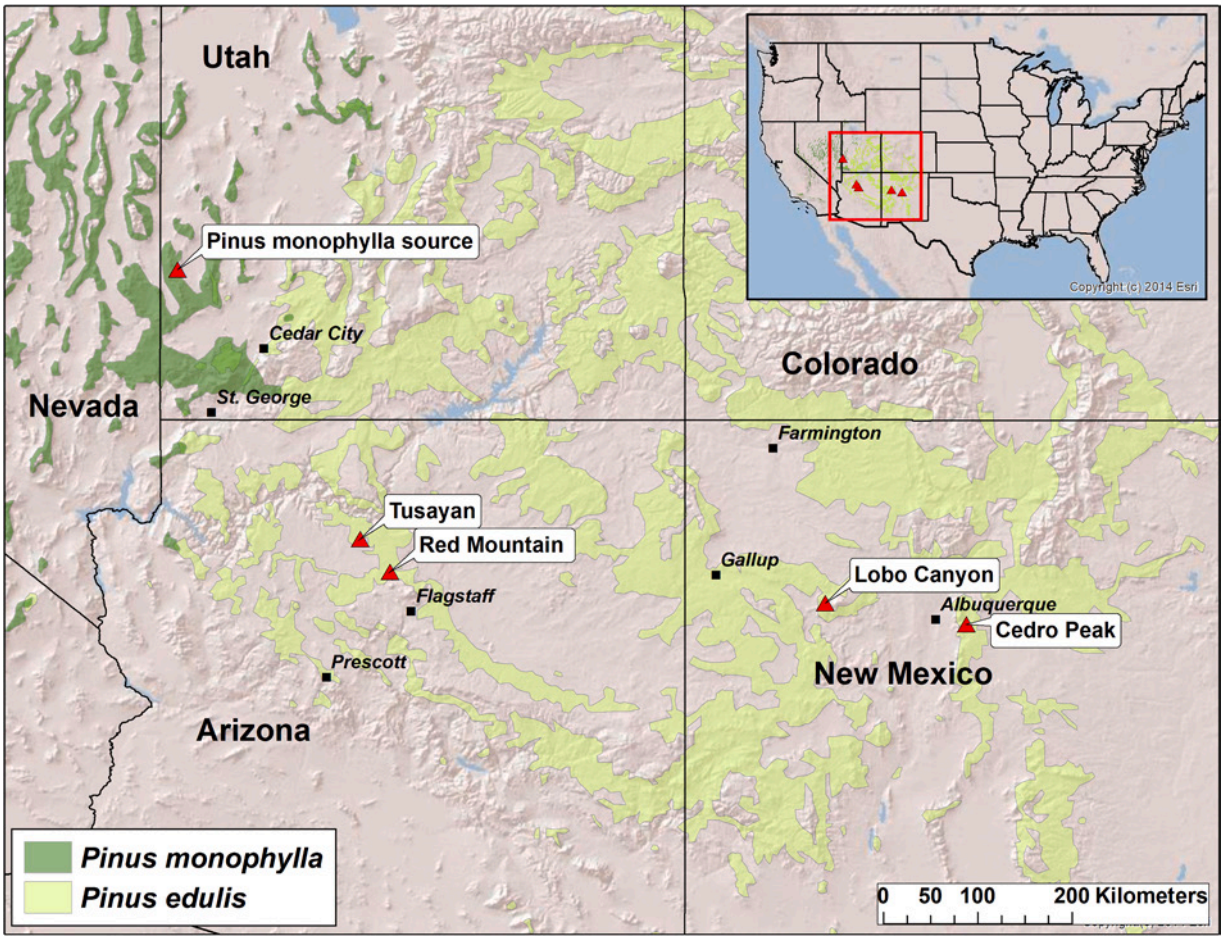

Fig. 1. Locations of field phenology sites and sources of pinyon ips beetles and host material for laboratory phenology testing. Lobo Canyon had two consecutive years of field data (2022, 2023) and is the source of *Pinus edulis* host material and beetles for laboratory studies. The other phenology sites had a single season of field phenology data collection (Red Mountain 2022, Cedro Peak 2023, Tusayan 2023).

emergence cages as described above. At Tusayan we baited three live *P. edulis* while at Cedro Peak we baited four live *P. edulis*. Data collection and caging of subsequent generation trees followed as described for the 2022 sites excepting that Tusayan had five passive traps and Cedro Peak had only two passive traps. Additionally, the Lobo Canyon site was used again with cages deployed on five trees with overwintering brood, five passive traps, and four baited live *P. edulis*. This site was re-established on 3 April 2023.

2.2. Phloem and air temperatures

To monitor phloem temperatures, i.e., beetle habitat, pheromone baited trees at the Lobo Canyon and Red Mountain sites in 2022, and Cedro Peak and Tusayan sites in 2023, were probed with thin-tipped (34 mm^2) thermocouples (Omega Engineering, Inc., Stamford, CT) placed into the phloem and attached to a datalogger (CR1000, Campbell Scientific, Inc., Logan, UT). Air temperature was also monitored at each site within a radiation shield using a temperature probe (Campbell Scientific probe 107) attached to the datalogger and/or a temperature recorder (HOBO datalogger, Onset Computer Corp., Bourne, MA). Air temperature, but not phloem temperature, was monitored at Lobo Canyon during 2023 (Fig. S1).

For empirical phenology model development and evaluation, daily maximum and minimum air temperatures for the interval from DOY 1 to the date of datalogger installation, for each site-year except Lobo Canyon 2023 which had continuous measurements from 2022, were modeled from nearby remote automated weather station (RAWS; https://mesowest.utah.edu/) data using a generalized linear mixed model (PROC GLIMMIX, SAS Institute, Inc., Cary, NC, USA; Littell et al., 2006). Covariates included season (Winter, Spring, Summer, and Fall) and the difference between daily maximum and minimum temperature at the RAWS. Hourly temperatures were then estimated using a sine-wave curve.

The mechanistic model (see 2.4.2) was developed with observed hourly phloem temperatures. To evaluate and run the model when only air temperatures are available, we modeled phloem temperatures using observed phloem and air temperatures from all site-years with covariates of "night" (2000–0600) and "early day" hours (0700–1500). For probed trees that were successfully attacked, we only used phloem temperature data when brood were developing in the tree because phloem temperatures in these trees could be confounded with foliar loss and bole desiccation. The phloem temperature model was fitted using least-squares linear regression (PROC REG, SAS Institute, Inc., Cary, NC, USA), with night and early day hours coded with dummy variables. Including "late day" hours did not appreciably improve model fit so we only use the three explanatory variables. The least-squares regression model for predicting phloem temperature from air temperature, regardless of bole aspect, is:

$$Phloem_{yhat} = 3.113 + 0.907(Air\,temperature) + 1.887(Night) - 2.555(Early) \quad (1)$$

where Night =1 if hour of day is 2000-0600, 0 otherwise; and Early=1 if hour of day is 0700-1500, 0 otherwise. R^2_{adj} of this model was 0.920.

Standard errors for model parameters: *Intercept* (0.064), *Air temperature* (0.002), *Night* (0.052), *Early* (0.049).

2.3. Phenology data - laboratory

Two each live and currently infested *P. edulis* were harvested from the Lobo Canyon site on 20 September 2022 and transported to the USDA Forest Service Rocky Mountain Research Station laboratory in Logan, UT. Infested trees contained brood ranging from late instars through newly-eclosed adults. Bolts with teneral adults were initially held in a walk-in cooler at near 0 °C while bolts with less mature brood were held in incubators at 20 °C (I-36VL, Percival Scientific, Inc., Perry, IA). When brood maturity was similar among all bolts, some bolts were held at 20 °C to allow brood adult emergence while others were held in the walk-in coolers until later use.

Emerging brood adults were sexed according to characters of dorsal portion of the head wherein female pinyon ips have a pars stridens-plectrum for stridulation whereas males lack this morphology (Lukic et al., 2021). On 24 October 2022, males were inserted into pre-drilled holes on uninfested bolts, spaced at ~5 cm and away from bolt ends. Flexible screening was stapled over the holes in an attempt to keep beetles from abandoning the log. The next morning, one female was inserted into the same holes and a second female was added during the afternoon. From 1–3 November 2022, bark was removed from bolts to collect eggs. We collected from the distal end of egg galleries to ensure the most recently laid eggs, and eggs were sorted by distance from the distal end in 1 cm increments. We favored eggs 0–1 cm distal when available and did not use any eggs >4 cm distal.

Using phloem peeled from uninfested *P. edulis*, we made phloem sandwiches with 10 eggs per sandwich, placing eggs into artificial niches in a regular pattern. The infested phloem was then held between glass and Plexiglas plates, 15 × 15 cm, with ventilation holes drilled into the Plexiglas (Bentz et al., 1991; Hansen et al., 2001). Medical tape was used to tightly secure the plates, holding the phloem to the glass as securely as possible, while allowing a degree of ventilation. We made seven plates each for 10, 15, 25, and 30 °C constant temperature treatments. Sandwiches were held vertically in a rack within a desiccator, the desiccator bottom containing a saltwater solution to maintain humidity near 95 %. Each desiccator was placed in an incubator (I-36VL, Percival Scientific, Inc., Perry, IA). To best mimic subcortical conditions, incubator lights were kept off and plates were held in constant darkness except during daily inspections (Hansen et al., 2001). Temperatures were monitored with a datalogger (CR1000, Campbell Scientific, Inc., Logan, UT) and adjusted to within 0.1 °C of the target temperature. Thereafter, phloem sandwiches were examined daily, within a 3-hour window, for molting and metamorphosis. Headcap exuviae were noted and assumed to be clear evidence of a molt since the previous observation. We also measured the headcap widths to construct a histogram to define the number of instars and determine breakpoints in the event of ambiguity among instars. These procedures were repeated for temperatures 8, 20, 32, and 34 °C with green bolts infested with males on 21 November 2022 and eggs collected and phloem sandwiches constructed 28–30 November 2022.

Additionally, we obtained bolts of live and infested *P. monophylla* from the Mountain Home Range, Utah on 7 November 2022 (38.434 N, 113.887 W, elevation 2142 m) (Fig. 1). Beetles and phloem from these trees were used to build phloem sandwiches held at two of the constant temperatures used in experiments with *P. edulis*, 25 and 30 °C. These sandwiches were constructed on 6 March 2023. Development time in phloem sandwiches of individuals from *P. edulis* and *P. monophylla* populations were compared using a generalized linear mixed model (PROC GLIMMIX, SAS Institute, Inc., Cary, NC, USA). As part of a separate experiment comparing pinyon ips brood success in *P. monophylla* and Great Basin bristlecone pine (*P. longaeva* Baily) (Bentz and Hansen, unpublished data), we monitored total time for brood development (infestation to brood adult emergence) in four *P. monophylla* bolts infested 18–25 January 2023 and held at constant 25 °C.

2.4. Modeling pinyon ips phenology

2.4.1. Empirical phenology model development

Adult emergence cage data from field sites (see Section 2.1) were summarized as cumulative proportions of total emergence per cage at each collection date. Cage data with fewer than 20 total beetles captured were not used in the model building described below. This included site-years where trees were not caged beyond those identified as having overwintering brood due to low numbers of attacks on baited trees (e.g., Tusayan 2023 and Red Mountain 2022 sites). Also, two cages intended to capture emerging brood from the overwintering generation had emergence coinciding with that of the first summer generation. It is likely those cages were deployed over unutilized phloem and overwintering generation beetles infested that material rather than a novel host; those data were censored during model building.

Independent empirical sub-models were created for spring emergence of the overwintering and summer generations, wherein we observed approximate dates of first attacks for the latter but not the former. Similar to Bentz et al. (2023) for *Dendroctonus brevicomis* LeConte, spring emergence was modeled using a cumulative Weibull distribution (minpack.lm package, nlsLM function) (Elzhov et al., 2016; R Core Team, 2022). The dependent variable was cumulative proportions of total emergence per cage per observation. Explanatory variables tested were air temperature-based cumulative hours and degree-hours above thresholds from 4–16 °C in 1 °C increments using a biofix starting on DOY 1. Cumulative proportions of emergence and temperature variables were matched by DOY. We used the residual standard error to determine the best-fitting variable. Results from this model were used to generate a temporal distribution of emergence for the overwintering generation. After selecting only cages with > 20 pinyon ips, as described above, we had data from 35 cages, and each site-year is represented for the overwinter generation. We randomly selected 28 (80 %) of these to parameterize the spring emergence model, reserving the remainder for validation.

Similarly, for the summer generations model, the dependent variable was cumulative proportions of total emergence per cage per observation and we modelled emergence using a cumulative Weibull distribution. Explanatory variables tested were air temperature-based cumulative hours and degree-hours above thresholds from 4–16 °C in 1 °C increments but using a biofix date of first observed attacks on a tree. Other than for Lobo Canyon 2022, the summer generation data were confounded by lack of attacks at some site-years, or we were unable to observe the dates of first attacks. Therefore, the summer generation model was parameterized with Lobo Canyon 2022 data, and summer generation cage data from other site-years was used for comparisons to model predictions. After selecting only cages with > 20 pinyon ips, as described above, Lobo Canyon 2022 had summer generation data from 43 cages and we randomly selected 35 (81 %) of these to parameterize the summer emergence model, reserving the remainder for validation.

Predictions of the annual number of generations at a site can be made by linking the overwintering spring emergence and summer generation sub-models. The biofix date for the spring emergence model was always DOY 1. The biofix date for initializing the first summer generation was the date of predicted 50th percentile emergence for the overwinter generation. Each subsequent summer generation was initialized using the date of 50th percentile emergence for the previous generation. The combined model was visually evaluated by comparing model output to field observations.

2.4.2. Mechanistic phenology model development

Models were fitted to the egg through pupal stages and oviposition and adult stages separately. Initially, observed and censored development times of egg through pupal life stages estimated in laboratory

constant temperature phloem sandwich experiments (see Section 2.3) were fit assuming a lognormal distribution following the protocols outlined by Régnière et al. (2012) and described in Appendix A. Censored observations in the development time data occur when the end or beginning of the life-stage was unobserved. There were two kinds of censored observations in our data: 1) individuals died between subsequent observations; and 2) the beginning of egg development was unobserved. Eggs were harvested from all locations along a gallery segment but only those eggs at the distal end of the gallery segment could be considered as recently oviposited (i.e., < 1 day old). The probability that development completed in the time interval was estimated separately for each type of censored data (Appendix A).

Estimated and observed development time data for egg through pupal stages were then fitted to a modified version of the Logan rate curve (Hansen et al., 2011),

$$r(T) = \psi\left[\left(e^{\omega(T-T_b)} - 1\right) - \left(e^{\omega(T_m-T_b)} - 1\right)e^{-(T_m-T)\Delta_m}\right]. \quad (2)$$

Here T_m represents the upper threshold for development, and T_b is a fitted parameter that adjusts the location of the lower threshold but is not the actual lower threshold, which must be determined computationally. Δ_m is the thermal width of the transition between the optimal development temperature and the upper threshold. The parameter ω captures the exponential acceleration of development as temperatures rise above the lower threshold, while ψ controls the rate of development at optimal temperature.

It is not possible to directly measure bark beetle oviposition and adult development rates using our phloem sandwich technique (see McManis et al., 2018; Hansen et al., 2024; Wangen et al., 2024). Therefore, to estimate times for oviposition and adult development we used total time from infestation to emergence at constant 25 °C (using data from four replicate *P. monophylla* bolts, see Section 2.3), fitted to a log-normal variance model, coupled with observed and censored data for the egg through pupal stages. The method is similar to that described by Wangen et al. (2024) for *D. ponderosae*. First, observed and censored development data for egg through pupal life stages were fitted to a modified Logan rate curve (Eq. (2); see Appendix A). The predicted development time from egg to pupa at 25 °C was subtracted from the observed emergence time from the four bolts, yielding an estimated distribution of times for combined oviposition and adult development. The fraction of time ascribed to either oviposition or adult development was then calibrated using field observations (see Appendix B for a full description).

A distribution model for phenology that includes oviposition through adult emergence was then compiled. Briefly, all individuals in each day starting a life stage are treated as a cohort whose emergence will follow a log-normal distribution with mean emergence time given by summing the rate curve over observed phloem temperatures. All cohorts within a stage are summed and aggregated daily to generate the predicted emergence distribution for the life stage (Régnière and Powell, 2013). The model was developed in MATLAB (Mathworks, Inc.) and was initiated using an initial attack modeled as a Gaussian distribution with standard deviation of three days and maximum attacks occurring six days after the first attack observation.

Preliminary comparisons of model output to Lobo Canyon 2022 cage data, with known dates of first attacks on trees, suggested the model was slow for this New Mexico population. Because we used data from a Utah population reared in *P. monophylla* to estimate oviposition and adult development rates, it is possible the Utah population has relatively slow *total* development rates despite minimal differences from egg through pupa. Therefore, we estimated a scaling parameter, S_A, to speed overall development time in the adult and ovipositional stages. This was accomplished using emergence cage data collected on north and south aspects of two Lobo Canyon 2022 baited trees with phloem temperature measurements and dates of first attacks observed within a four-day window. To maximize correspondence between predicted and observed timing, we minimized the sum square error between the timing of observed and predicted quantiles of emergence. Mathematically, we calculated timing error for given S_A, f_O as

$$E(S_A, f_O) = \sum_{\text{Tree/Aspect}} \sum_{n=1}^{N_j} [t_n - \hat{t}_n]^2, \quad (3)$$

where t_n is an observation day for a given tree/aspect and $\hat{t}_n$ is the predicted day on which predicted cumulative emergence from the phenology model was equal to cumulative observed emergence on day t_n. Tree/aspect are indexed by j, with N_j observations on each tree/aspect. The unknown parameters were determined by minimizing $E(S_A, f_O)$ using the Nelder-Mead Simplex Method (function fminsearch in MATLAB, Mathworks, Inc.).

2.5. Simulating pinyon ips phenology

The empirical phenology sub-models, for the overwinter and summer generations, are driven by hourly air temperature data (see Section 2.4.1). The biofix date for the overwinter spring emergence model was always DOY 1. The biofix date for initializing the first summer generation was the date of predicted 50th percentile emergence for the overwinter generation. Each subsequent summer generation was initialized using the date of 50th percentile emergence for the previous generation.

The mechanistic phenology model was developed using constant temperature laboratory data (see Section 2.3) and field-observed phloem temperatures (see Section 2.4.2) and, therefore, is driven by phloem temperatures. We used predicted hourly phloem temperatures for model simulations and evaluation (see Section 2.2). In our simulations, the first summer generation was started when the 15th percentile overwinter beetle emerged as predicted by the empirical spring emergence sub-model. Thereafter, each generation was likewise started using the date of 15th percentile beetle emergence of the previous generation. This degree of emergence for starting a new generation was chosen after comparing observed dates of cumulative emergence with observed dates of first attacks. That is, observed dates of first attacks on new trees in field data roughly corresponded with 15 % observed cumulative emergence from previously infested trees. The 15th percentile emergence threshold also resulted in better model fit when compared to other thresholds (e.g., 20th, 25th percentile).

Both models were also used to predict the potential range in number of generations per year for exceptionally cold and warm sites-years. For a cold site-year, we picked a location from the northern extent of *P. monophylla* range near Hardware Ranch, UT (41.566 °N; 111.496 °W) (Little, 1971; http://www.usgs.nau.edu/global_change/RangeMaps.html) and used 1993 as the year (one of the coolest summers on record for northern Utah; https://wrcc.dri.edu). For a warm site-year, we picked a location from the Guadalupe Mountains, TX (31.917 °N; 104.834 °W) and picked 2017 as the year (among the warmest years on record in the Southwest). Daily maximum and minimum temperatures for each location were derived from Daymet interpolations (https://daymet.ornl.gov/) and fitted to a sine-wave curve to get hourly temperatures. For the mechanistic phenology model, hourly phloem temperatures were estimated from air temperatures as described above (Section 2.2).

3. Results

3.1. Phenology - field sites

Passive trap and emergence cage data suggest pinyon ips populations were highest at Lobo Canyon 2022, compared to all other sites (Table 1, Fig. 2). At each site-year, we observed some adult emergence soon after site installation in late March, but peak spring emergence of the overwinter generation generally occurred mid-April to early May, DOY

Table 1
Total number of emergence cages and trees caged and passive traps deployed at each site-year. Total number of pinyon ips adults caught in cages and traps are also shown. Individual cages and traps were deployed throughout a summer to capture generation timing (see Fig. 2).

Site-year	No. cages (no. trees): No. pinyon ips	No. passive traps: No. pinyon ips
Lobo Canyon 2022	57 (25): 6635	6: 368
Lobo Canyon 2023	12 (9): 878	5: 17
Cedro Peak 2023	10 (6): 1782	2: 4
Red Mountain 2022	10 (6): 2735	6: 55
Tusayan 2023	2 (1): 171	5: 11

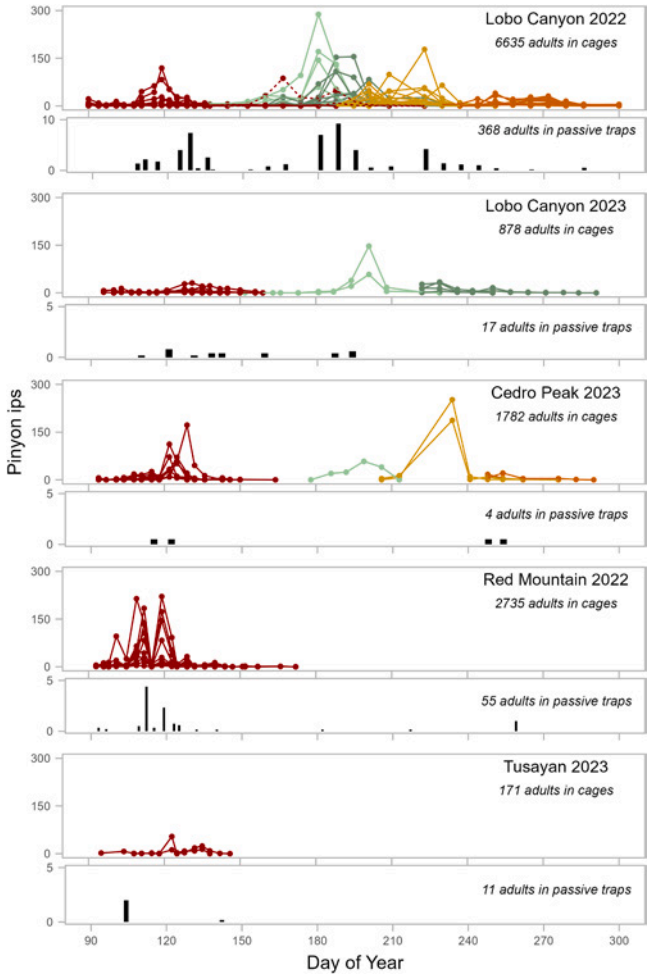

Fig. 2. Adult pinyon ips emergence per tree cage and mean number of adults caught in passive traps at five site-years in New Mexico and Arizona. Colors at a site-year represent catches for cages grouped by attack date. Cohorts in cages representing each summer generation were often confounded by parent beetles infesting unused phloem under cages and, in some cases, delays in attacks on baited trees by a full generation. Adults caught in cages over two generations are indicated by a dotted line. See Table 1 for numbers of cages, trees caged, and passive traps at each site-year.

105–130 (Fig. 2). Some cages deployed during mid-summer captured the 50th percentile adult in as few as 19 days after observed date of first attacks, demonstrating the potential for pinyon ips to produce multiple generations per year depending on temperatures. Passive traps caught the most pinyon ips adults at Lobo Canyon 2022, and the trend in catches generally followed that of emerged adults in tree cages. The number of emerged adults had generally declined by the last observed summer generation (Fig. 2).

At Lobo Canyon 2022, emergence cage data suggest three and at least a partial fourth generation occurred during the calendar year, although there was extensive cohort overlap among generations potentially due to re-emergence of parent adults. This site had the greatest number of tree cages deployed throughout the summer (Table 1). Emergence from two cages on overwinter trees at Lobo Canyon 2022 coincided with emergence of the first summer generation suggesting that parents may re-emerge and initiate a new cohort in unused phloem on natal trees (Fig. 2). Emergence cages left on the third summer generation trees at Lobo Canyon 2022 were checked the following spring and none of the cages captured additional beetles (2023, DOY 93). This suggests the third generation may have been complete in that cohort splitting did not occur over the winter, although potential overwinter mortality under bark was not investigated. Additionally, two trees were identified with dates of first attack on DOY 279 and 280 suggesting either re-emerged parents or attacks by emerging third generation beetles. Cages were installed on these trees but no brood emerged during 2023 indicating unsuccessful attacks or brood mortality during winter. Cage data at Lobo Canyon 2023 and Cedro Peak 2023 also suggest three and possibly four generations occurred. Spring emergence of the overwinter generation occurred at Red Mountain 2022 and Tusayan, 2023, but no additional generations were observed in emergence cage or passive trap data.

3.2. Phenology – laboratory

We observed three pinyon ips larval instars, with obvious breakpoints between instars, similar to other *Ips* species (Wilkinson et al., 1963; Ostmark, 1966; Baier et al., 2007) (Fig. 3). Developmental rates were relatively fast; the sum of mean life-stage-specific times from egg through adult eclosion was 29 days at 20 °C (Fig. 4). At 32 °C, three individuals molted twice between the ~24 h observations, indicating our temporal resolution was inadequate for such rapid development. Very little development was observed at 8 °C. Seven eggs hatched at that temperature, but all were collected 1–3 cm from the distal gallery ends. That is, some unknown amount of development occurred at 20 °C before the eggs were transferred to 8 °C. The censored data indicate instar 1 development at 8 °C but we otherwise did not observe development at this temperature. At the other extreme, 34 °C, development time was only slightly slower than at the optimal 30–32 °C (Fig. 4). There is anecdotal evidence that 34 °C is close to the upper developmental threshold in that we saw increasing mortality among relatively mature brood. At 30 °C all instar 3 and pupae survived to adult eclosion whereas two individuals died before eclosion at 32 °C and seven died at 34 °C.

Pinyon ips from *P. monophylla* developed faster than those from *P. edulis* in the egg (collected 1–2 cm distal from gallery ends) ($F_{1,\ 48} = 14.27$; $p < 0.001$) and instar 3 ($F_{1,\ 68} = 24.44$; $p < 0.001$) life stages. *Pinus edulis*-sourced instar 2, however, were marginally ($F_{1,\ 68} = 3.92$; $p = 0.052$) faster than *P. monophylla*-sourced instar 2. We found no

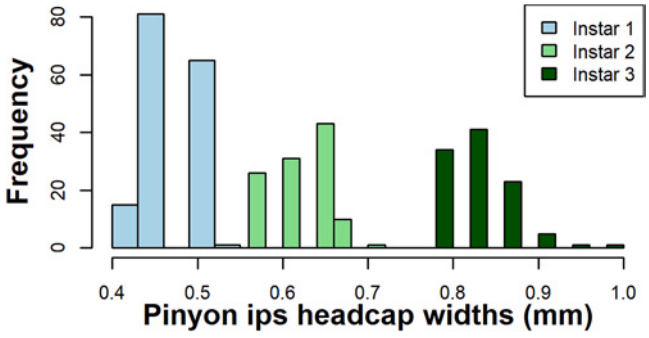

Fig. 3. Histogram of pinyon ips larval headcaps widths, measured with a dissection scope at 25X. This distribution along with observed headcap exuviae, between molts, indicate three instars for this organism. These data are from the phloem sandwiches at 10, 15, 25, and 30 °C constant temperature treatments.

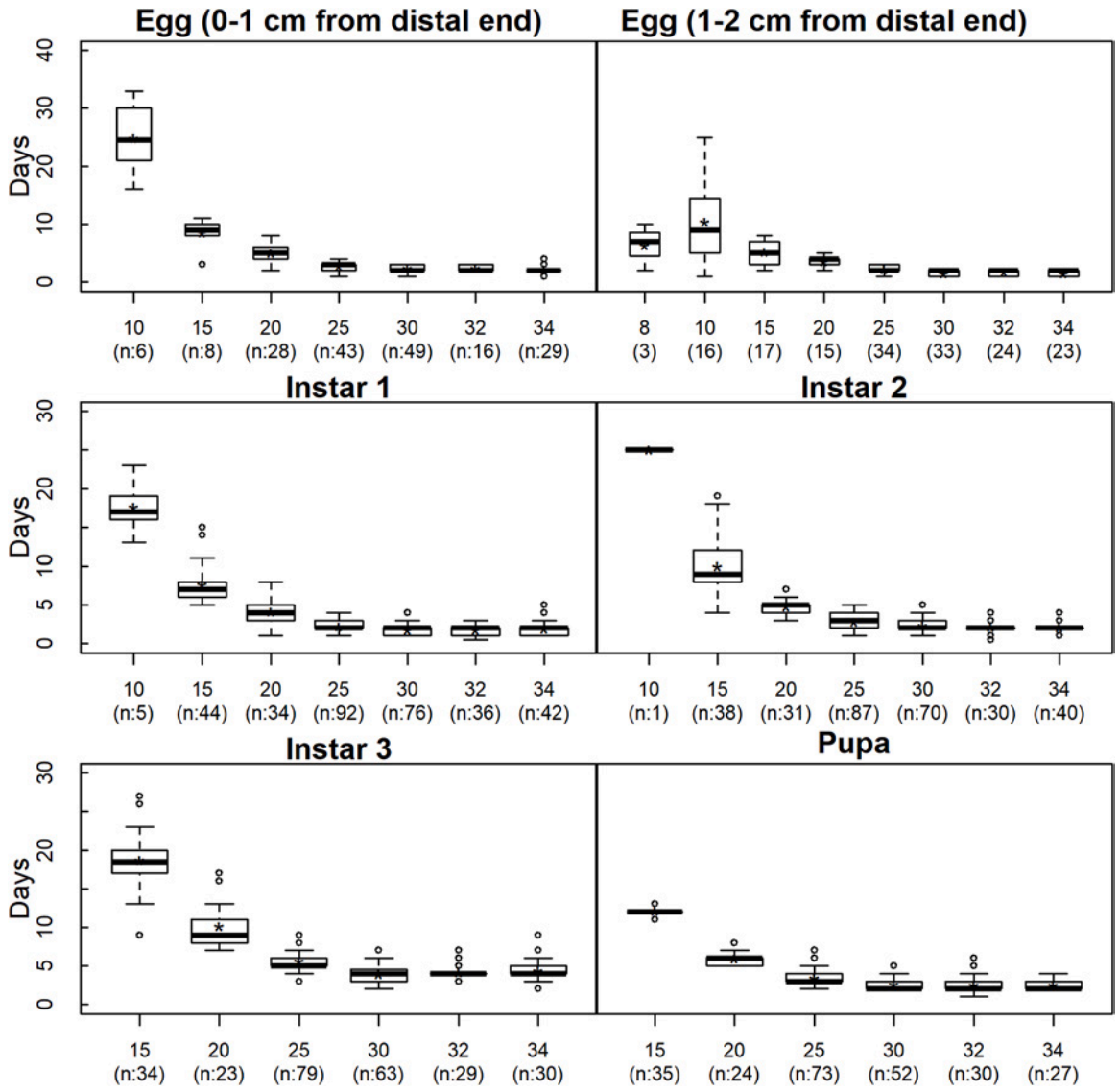

Fig. 4. Time to complete each pinyon ips life stage at temperatures from 8–34 °C. Eggs that were collected 0–1 cm from the distal end of the gallery were more likely to not have developed measurably prior to collection, compared to eggs collected 1–2 cm from distal end. Sample size, n, is shown in parentheses.

significant differences among the hosts for other life-stages. Differences among host trees for specific life-stages, however, resulted in very little differences in overall time from egg to pupa. The sum of mean times from eggs (collected 0–1 cm distal) through pupa at 25 °C was 15.04 days for *P. monophylla* beetles and 15.84 days for *P. edulis* beetles. At 30 °C, the sum of mean times for *P. monophylla* beetles was 11.33 days whereas *P. edulis* beetles took 12.20 days. We therefore used pooled data from both host trees for development of the egg through pupa stages of the mechanistic phenology model.

3.3. Modeling pinyon ips phenology

3.3.1. Empirical phenology model

We used independent air-temperature based models to account for differences among the overwintering and summer generations. For overwinter generation emergence, cumulative counts of hours above the various thresholds generally had lower residual standard hours than cumulative degree-hours above the thresholds. Cumulative hours ≥ 13 °C from DOY 1 was found to be the best fitting predictor variable (Fig. 5a). This result is supported by notable increases in observed development rate of multiple lifestages between 10° and 15 °C in constant temperature laboratory experiments (Fig. 4). The cumulative proportion of emerged beetles is given by:

$$P = 1 - \exp\left(- (CH13/297.969)^{2.185} \right), \quad (4)$$

where *CH13* is the cumulative hours ≥ 13 °C. Thus, the 50th percentile overwinter beetle is predicted to emerge after 252 cumulative hours ≥ 13 °C, starting on DOY 1. Data reserved for validation appear to be well-represented by this model. Median emergence of reserved data is close to model predictions albeit the reserved data suggest the curve could be steeper (Fig. 5a). Examining the validation data, model predictions explained 85 % of the variation for spring emergence (adjusted $R^2 = 0.853$, $F_{1,150} = 879$, $p < 0.001$).

For summer generations emergence, cumulative counts of hours above the various thresholds also generally had lower residual standard hours than cumulative degree-hours above the thresholds, and cumulative hours ≥ 13 °C was found to be the best fitting predictor variable (Fig. 5b). The cumulative proportion of emerged beetles is given by:

$$P = 1 - \exp\left(- (CH13/996.328)^{3.886} \right); \quad (5)$$

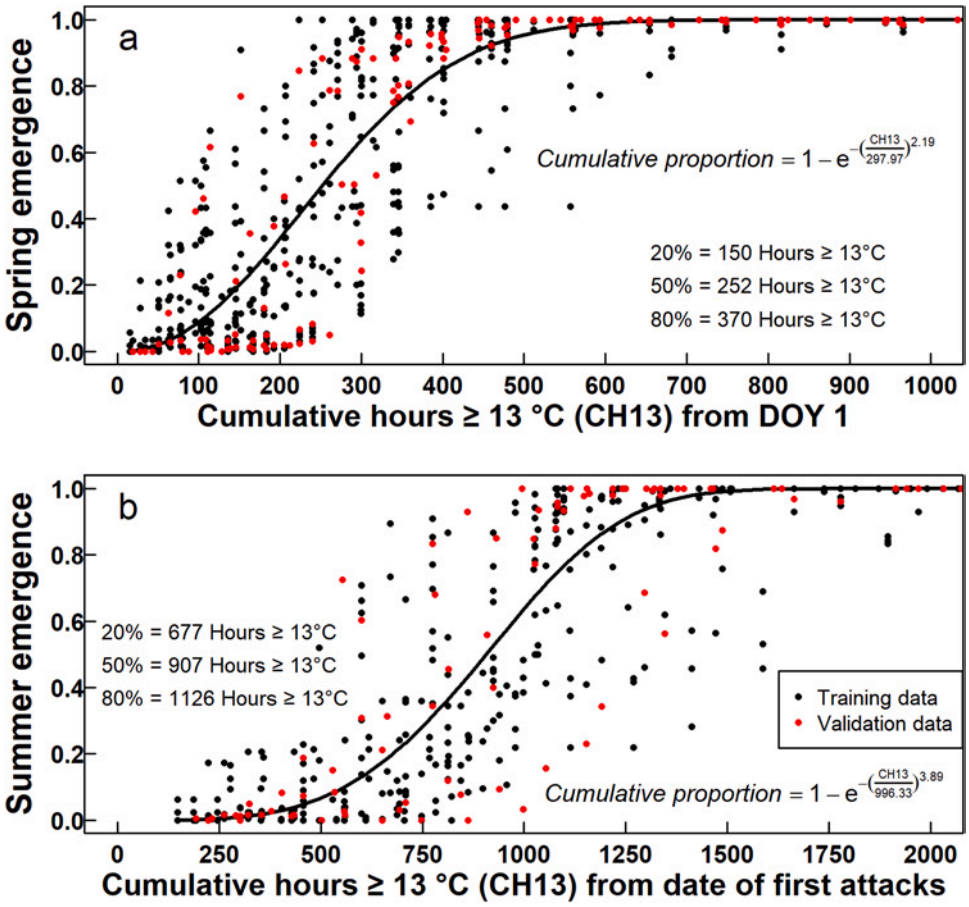

Fig. 5. (a) Spring emergence model training and validation observations as a function of cumulative hours ≥ 13 °C from the first day of the year, with the modeled Weibull distribution (black trace). (b) Summer generation model training and validation observations as a function of cumulative hours ≥ 13 °C from the date of first attacks on the caged trees, with the modeled Weibull distribution (black trace).

where *CH13* is the cumulative hours ≥ 13 °C. Thus, the 50th percentile summer generation beetle is predicted to emerge after about 907 cumulative hours ≥ 13 °C starting from field-observed dates of first attack. Examining the validation data, model predictions explained 73 % of the variation for summer emergence (adjusted $R^2 = 0.732$, $F_{1,87} = 879$, $p < 0.001$).

3.3.2. Mechanistic phenology model

Parameter estimates of observed and censored development time for each life stage (i.e., egg, instar 1, instar 2, instar 3, and pupa) individually fitted to a modified Logan rate curve, and the five life stages pooled and then fitted to the same Logan rate curve, are shown in Table C.1. For the pooled model, which was used to estimate oviposition and adult rates, model fit was good, $R^2 = 0.946$, when only the median of possible emergence windows and egg data only from 0–1 cm from the distal end of the gallery (i.e., recently oviposited) were included in calculating accuracy (see Appendix C, Fig. C.2). The lognormal model for oviposition to brood adult emergence, based on constant temperature bolt data, was also a suitable fit (Fig. C.3). The combined oviposition/adult development curve was parsed to reflect oviposition and adult development separately. The amount ascribed to oviposition, f_O, was estimated as 0.6122. Thus, the fraction ascribed to adult development was 1 – 0.6122 (see Appendix C). Additionally, because model comparison with emergence cage data indicates there is likely a regional difference in overall developmental timing (i.e., New Mexico beetles reared in *P. edulis* versus Utah beetles reared in *P. monophylla*), we also included a scaling parameter, S_A, to adjust overall development time in the adult and ovipositional stages. Scaling each of the oviposition and adult stages to minimize least square differences compared to emergence cage data for two Lobo Canyon 2022 trees and using observed dates of first attacks and measured phloem temperatures to drive the model, S_A was estimated as 1.1205 (Fig. C.7).

3.4. Simulation of pinyon ips phenology

The timing and number of pinyon ips generations were predicted using an empirical spring emergence model for the overwinter generation that was coupled with an empirical model for summer generations. Predictions were also made using a mechanistic model developed using laboratory data on life stage specific development, that was initiated each summer using predictions of spring emergence from the empirical sub-model. Observed temperatures at each site were used to run the models (Fig. S1). The empirical spring emergence model well-fit observed emergence cage data at all five sites, with between 0- and 5-days difference between median emergence predictions and median observed emergence in tree cages (Table 2, Fig. 6). At sites with adequate data, passive traps were also in alignment with cages and predictions from the empirical and mechanistic models for the overwinter and first summer generations (Figs. 2, 6). At Lobo Canyon 2022 and 2023, median emergence predictions for the first and second summer generations differed by 1 day at most between the two models, and there were only 3- to 5-days difference between model predictions and tree cage observations (Table 2, Fig. 6). Predictions for median emergence of the first summer generation at Cedro Peak 2023 were also identical between the two models (Table 2).

Predictions and relationships with observed cage data for

Table 2
Day of year (DOY) pinyon ips median emergence predictions from the empirical spring (overwinter generation) and summer generations models and the mechanistic model for summer generations. Also shown are the estimated DOY pinyon ips median emergence observed for tree cages in each generation (see Fig. 2). Only the empirical model was used to predict the overwinter generation. At Cedro Peak 2023 baited trees were not sufficiently attacked and unused phloem under cages was re-infested, resulting in inconsistent data. No pinyon ips were observed in cages other than the overwinter generation at Red Mountain 2022 and Tusayan 2023.

Site-year	Generation	Empirical models	Mechanistic model	Tree cages
Lobo Canyon 2022	Overwinter	119	–	119
	1st summer	180	180	183
	2nd summer	221	221	208
	3rd summer	265	–	260
Lobo Canyon 2023	Overwinter	130	–	129
	1st summer	190	190	195
	2nd summer	230	228	226
	3rd summer	292	295	–
Cedro Peak 2023	Overwinter	121	–	123
	1st summer	177	176	–
	2nd summer	215	206	–
	3rd summer	253	241	–
	4th summer	292	282	–
Red Mountain 2022	Overwinter	106	–	111
Tusayan 2023	Overwinter	121	–	125

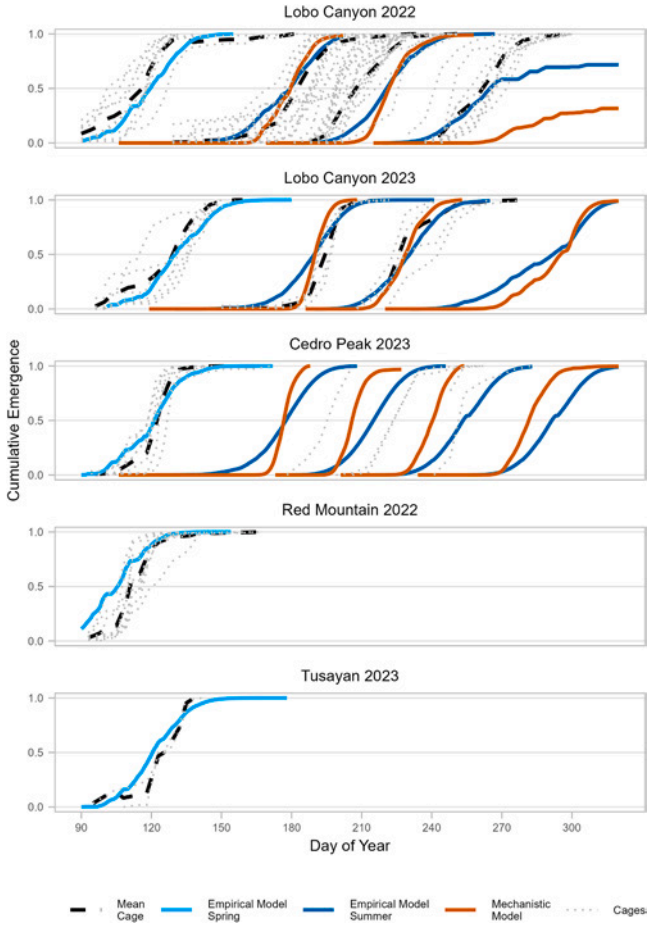

Fig. 6. Cumulative emergence of pinyon ips observed in tree emergence cages compared to predictions from the spring and summer empirical models and summer generations from the mechanistic model at five site-years. Mean cage observations are the average number of pinyon ips in emergence cages estimated for each generation. Also shown are data for each individual cage.

generations after the second summer generation were less synchronized. At Cedro Peak 2023 cage data did not coincide with predictions from either model, likely because the few cages sampled captured re-emerged parents rather than brood adults. At Lobo Canyon 2022, empirical model predictions suggest that ~70 % of the third summer generation had sufficient heat to emerge and ~30 % adult emergence was predicted from the mechanistic model. Some proportion of third summer generation adults emerged into tree emergence cages, however, and no adults were observed in cages the following summer suggesting a complete generation. It is important to note, however, that potential mortality of individuals under bark was not investigated. Predictions of median emergence timing from the empirical and mechanistic models for the third summer generation at Lobo Canyon 2023 only differed by 3 days and both models predicted 100 % emergence that year. Third generation emergence cages are not shown because they were not checked the following spring at this site, and it is therefore unknown if the last summer generation was complete or partial. At Cedro Peak 2023, the warmest of the sites with summer generation cage data (3903 hrs > 13 °C) (Fig. S1), median emergence predictions from the two models differed by 12 and 10 days for the third and fourth summer generations, respectively (Table 2).

Using Daymet temperature interpolations of daily maxima and minima and a sine-wave curve to model hourly temperatures near Hardware Ranch, UT for 1993 (a cool site-year), the empirical models predicted median emergence of the overwinter generation on DOY 152 (June 1) and DOY 246 (September 3) for the first summer generation, but there was insufficient thermal input for a second summer generation. The mechanistic model, using phloem temperatures derived from these same air temperature data, predicted median first summer generation emergence to occur 22 days later than the empirical model (DOY 268, September 25), but similar to empirical model predictions, a second summer generation was predicted to not occur. For the Guadalupe Mountains location, 2017 (a warm site-year), the empirical models predicted four complete summer generations and a partial fifth generation whereas the mechanistic model predicted 68 % of a fourth summer generation would occur. At the warm site-year, therefore, the mechanistic model predicted slightly less development of a fourth generation than the empirical models.

4. Discussion

Our field data confirms that pinyon ips is multivoltine, capable of completing a generation in less than one month during the warmest time of year. Compared to laboratory-based constant temperature development data observed for other bark beetles, pinyon ips development at 25 °C is faster than other *Ips* species (Wermelinger and Seifert, 1998) and several *Dendroctonus* species (Wagner et al., 1984; Hansen et al., 2001; Régnière et al., 2012), resulting in the rapid generation times observed in our field data. An overwinter and two summer generations, with at least a partial third summer generation, were observed in the field, although pinyon ips numbers in traps and emergence cages had declined greatly by the last summer generation. Population size was also lower in 2023 than 2022 likely due to near-record precipitation during the winter 2022–23 removing much of the southwest US from drought classification by May 2023 (https://droughtmonitor.unl.edu/Maps/CompareTwoWeeks.aspx). As a species that attacks drought-stressed trees, the wetter than average weather likely contributed to declining pinyon ips populations (Raffa et al., 2008). These relatively wet conditions were particularly prevalent in northern Arizona where neither site-year had adequate attacks to initiate a successful summer generation, even on baited trees.

Spring emergence of the overwinter generation was relatively synchronous across sites in both 2022 and 2023, with clear separation from subsequent summer generations (Fig. 2). Low temperatures overwinter can homogenize spring emergence of populations by synchronizing development among individuals (Bjørnstad et al., 2016). As summer

progressed, however, emergence became more diffuse with less clear separation among generations, particularly at Lobo Canyon 2022, the site with the most sampled trees and emergence cages. Developmental asynchrony in multivoltine populations can occur due to multiple factors and in general the more summer generations, the greater the opportunities for smoothing of generations with less separation (Bjørnstad et al., 2016). Environmental variation among microhabitats can increase cohort overlap, and indeed, temperatures around the bole of a single infested pinyon pine varied by up to 3 °C during the warmest part of the day (Fig. S1a). Developmental asynchrony could also have been enhanced by the extensive developmental variation in egg through pupal lifestages that we observed in laboratory experiments (Figs. C.1, C.2). An extended oviposition period is another factor known to increase cohort overlap. In our field data, the oviposition period was lengthened when parent adults either re-emerged to colonize a new tree following initial oviposition or colonized unutilized phloem in the same tree. Re-emergence of parent adults for new attacks and gallery initiation is common among some *Ips* and *Dendroctonus* species (DeLeon et al., 1934; Coulson et al., 1978; Baier et al., 2007). These factors all likely contributed to cohort overlap and a smearing of generations (Bjørnstad et al., 2016).

Empirical sub-model predictions of spring emergence well-described observed emergence of caged trees not only at the site where model parameters were derived (Lobo Canyon 2022), but also at the four other monitored sites. Predicted median emergence was on average within 2.4 days of observed overwinter emergence from caged trees and timing of passive trap catches across the five sites. The first and second summer generations were also well-predicted by both the empirical model and the summer mechanistic model. Median emergence day predictions from the two models at Lobo Canyon 2022 and 2023 were within a few days. By the third summer generation, predictions from the two models diverged with each other, particularly at Lobo Canyon 2022 where mechanistic model predictions were much delayed relative to the empirical model. Predictions by the two models at Cedro Peak 2023, the warmest of the sites, differed by increasingly larger numbers of days after the first summer generation but then declined again by the fourth summer generation. Temperatures at Cedro Peak 2023 were warmer than Lobo Canyon 2022 (Fig. S1 b,c) where empirical model parameters were developed. These results, in addition to trends seen in model runs for the case studies (a cool Utah and warm Texas site), highlight how the mechanistic model predicted faster development in the warm mid-summer temperatures. This could be because the mechanistic model treats oviposition as a pulse, rather than a distribution, likely understating natural variance added during oviposition as was captured in the empirical model. Additionally, we have no observations of adult stage development in the laboratory and that stage was inferred using egg – pupae data and oviposition to adult emergence in bolts. Data regarding lower and upper thresholds for adult development would likely reduce uncertainty and improve model fit.

Despite not matching the exact timing of summer generations (after the second generation), the total number of summer generations predicted by both models generally corresponded with the generations observed in field data, except for a third summer generation at Lobo Canyon 2022. Predictions from both models suggested only a partial number of adults would emerge, with the remaining overwintering to emerge the following year. This type of adaptive plasticity, e.g. cohort splitting over winter, is not uncommon in animals (Crowley and Hopper, 2015). Although no individuals were observed in Lobo Canyon 2022 cages the following summer, winter mortality could have occurred, masking the fact that only a partial third summer generation occurred as predicted by both models. Predictions from both models for Lobo Canyon 2023 indicate completion of a third summer generation by the end of fall, and the warmer Cedro Peak 2023 site was predicted to complete a fourth summer generation, although field data is not available for comparison with these results. In the two case studies exploring predictions in a changing climate, both models predicted 2 annual generations at a cool site and up to 5 generations at a warm site. Our field data and model results therefore support Chansler (1964) and Eager (1999) who proposed 2–5 generations per year for pinyon ips depending on weather and site. Additionally, our finding of accelerated phenology in warmer conditions has also been found for other multivoltine bark beetle species including *I. typographus* (Potterf et al., 2025) and *D. brevicomis* (Robbins et al., 2022; Bentz et al., 2023).

Empirical and mechanistic models can complement each other (Tran et al., 2020), and we used the empirical spring emergence model to initiate summer generation simulations of the mechanistic model. Although the empirical models will be easiest to use, the mechanistic model provides a functional representation of the relationship between temperature and pinyon ips development and extrapolation to other areas may provide more realistic results than empirical models that were developed using field data from a single site. Additional field observations from multiple sites are needed for a comparative analysis of both models, key aspects of Good Modeling Practice (Jakeman et al., 2024).

Our pinyon ips empirical and mechanistic models both correctly predicted the number of summer generations at field sites with sufficient observed data. Field data and models indicate that pinyon ips is capable of two to five or more generations per year depending upon site temperature. The warmer temperatures needed to drive 5 annual generations likely have additive effects on host susceptibility in that heat contributes to drought stress on host trees (Gaylord et al., 2013; 2015). We expect pinyon ips outbreaks to become more frequent, if not more severe, as climate warming continues. Pinyon pines are typically not managed for timber, and treatments and thinning are often done for other resources including wildlife habitat. Large woody debris (i.e., slash) suitable for pinyon ips development that is created during pinyon pine treatments is currently managed following guidelines developed for *P. ponderosa* (DeGomez et al., 2014). These guidelines propose that treatments and slash creation should occur in the fall when temperatures are too cool for pinyon ips adult flight and attacks, also providing time for the slash to dry out and become unsuitable for beetle development the following spring. Our models, however, suggest under current and future climate the seasonal window for adult flight and attacks will expand, thereby reducing the management window for creating slash. The practical window for slash management may already be reduced in some areas, for example the Guadalupe Mountains, TX, where our models predict pinyon ips is likely active through November and beginning again in February. In addition to potential use for landscape-scale risk assessments similar to models based on PHENIPS developed for *I. typographus* (Baier et al., 2007; Pirtskhalava-Karpova et al., 2024), our models offer a method to define an appropriate slash management interval given a record of contemporaneous temperatures.

CRediT authorship contribution statement

E.M. Hansen: Writing – review & editing, Writing – original draft, Methodology, Investigation, Formal analysis, Data curation, Conceptualization. **J.A. Powell:** Writing – review & editing, Writing – original draft, Methodology, Formal analysis. **A. Graves:** Writing – review & editing, Project administration, Methodology, Investigation, Funding acquisition, Conceptualization. **S. Souder:** Writing – review & editing, Investigation, Data curation. **J.C. Vandygriff:** Writing – review & editing, Investigation, Data curation. **M. Gaylord:** Writing – review & editing, Investigation, Data curation, Conceptualization. **J. McMillin:** Writing – review & editing, Investigation, Data curation, Conceptualization. **B.J. Bentz:** Writing – review & editing, Writing – original draft, Supervision, Project administration, Methodology, Investigation, Funding acquisition, Formal analysis, Data curation, Conceptualization.

Declaration of competing interest

The authors declare that they have no known competing financial interests or personal relationships that could have appeared to influence

the work reported in this paper.

Acknowledgements

We are grateful for considerable assistance from Joe Beman (Cedro Peak data collection) and Emma Elsner (Tusayan data collection). Funding was provided by the USDA Forest Service Rocky Mountain Research Station and State, Private, and Tribal Forestry. The use of trade or firm names in this paper is for reader information only and does not imply endorsement by the U.S. Department of Agriculture of any product or service. The findings and conclusions in this publication are those of the authors and should not be construed to represent any official USDA or U.S. Government determination or policy.

Supplementary materials

Supplementary material associated with this article can be found, in the online version, at doi:10.1016/j.ecolmodel.2025.111282.

Appendix A

A. 1 Fitting egg through pupa lifestage development

For fitting observed and censored development times of the egg through pupal lifestages, we follow the protocols outlined by Régnière et al. (2012), which assumes lognormal distribution of development times in a population, that is

$$t = \delta\tau(T,\Theta), \tag{A.1}$$

where t is an individual's time to emergence at a constant temperature, T, τ is the theoretical development time at this temperature, Θ is a vector of parameters, and δ is a random variable with mean one and lognormal distribution,

$$\delta = e^{\epsilon},\ \epsilon \sim N\left(-\frac{1}{2}\sigma^2,\ \sigma^2\right). \tag{A.2}$$

Here σ^2 is the variance of the exponentiated random variable, ϵ. Offsetting the mean of the normal distribution by $\frac{1}{2}\sigma^2$ is necessary to force the mean of the multiplicative variance to be one after exponentiation (Mangel and Hilborn, 2013). Predicted development times are the inverse of the theoretical rate of development,

$$r(T,\Theta) = \frac{1}{\tau(T,\Theta)}, \tag{A.3}$$

and therefore, the probability that an individual will complete development *before* time t is given by

$$P(\text{ Development completes before} \le t) = \Phi\left(\log[t\ r(T,\Theta)], -\frac{1}{2}\sigma^2,\ \sigma^2\right). \tag{A.4}$$

Here the function $\Phi(\cdot,\mu,\ \sigma^2)$ denotes the cumulative density function of the normal distribution with mean μ and variance σ^2.

It is unlikely to observe an egg hatch or larval molt. More realistically, observations are made on some schedule and what is known is that individual i completed development at temperature T_j in the time interval $(t_{i,j} - \Delta t_{i,j},\ t_{i,j})$, where $t_{i,j}$ is the first observation after eclosion or molting and $\Delta t_{i,j}$ is time lapsed since the previous observation. If we denote $q_{i,j}$ as the probability of observing a life stage transition in the given interval, then we can use the difference between cumulants at the interval endpoints to write

$$q_{i,j} = \Phi\left(\log\left[t_{i,j}\ r(T_j,\Theta)\right], -\frac{1}{2}\sigma^2,\ \sigma^2\right) - \Phi\left(\log\left[(t_{i,j} - \Delta t_{i,j})\ r(T_j,\Theta)\right], -\frac{1}{2}\sigma^2,\ \sigma^2\right). \tag{A.5}$$

Note that $\Delta t_{i,j}$ varied among observations, even at the same temperature, because the individual may have been submerged in the phloem sandwich at either the beginning or end of development, and so this uncertainty is added to the length of the observation window.

A.2 Censored data

A censored observation occurs when the end (or beginning) of the lifestage was unobserved. We treat censored observations as time intervals with an infinite upper limit (so $\Phi = 1$). There were two kinds of censored observations in our data. In the simplest case, individuals died between subsequent observations, so the last time they were observed alive was $t_{i,j} - \Delta t_{i,j}$, which must underestimate their time of development. Then the probability that development completed in the time interval $(t_{i,j} - \Delta t_{i,j},\ \infty)$, $q^d_{i,j}$, would be

$$q^d_{i,j} = 1 - \Phi\left(\log\left[(t_{i,j} - \Delta t_{i,j})\ r(T_j,\Theta)\right], -\frac{1}{2}\sigma^2,\ \sigma^2\right). \tag{A.6}$$

In the second case, for some eggs the beginning of development was unobserved, because eggs were harvested from all locations along a gall segment but only those eggs at the distal end of the gall segment could be considered as recently oviposited. Because the time of oviposition is unknown, all that can be said with certainty is that development would have completed in the time interval $\left(t_{i,j} - \Delta t_{i,j},\ \infty\right)$. The probability of development during this interval, $q_{i,j}^{gs}$ (like that for observations censored by death), would be.

$$q_{i,j}^{gs} = 1 - \Phi\left(\log\left[\left(t_{i,j} - \Delta t_{i,j}\right) r\left(T_j, \Theta\right)\right], -\frac{1}{2}\sigma^2,\ \sigma^2\right). \tag{A.7}$$

For each lifestage, the negative log likelihood is then

$$NLL(\Theta) = -\sum_{i,j}\left[\left(1 - \delta_{i,j}^{d} - \delta_{i,j}^{t} - \delta_{i,j}^{gs}\right)\log\left(q_{i,j}\right) + \delta_{i,j}^{d}\log\left(q_{i,j}^{d}\right) + \delta_{i,j}^{t}\log\left(q_{i,j}^{t}\right) + \delta_{i,j}^{gs}\log\left(q_{i,j}^{gs}\right)\right]. \tag{9}$$

Here the δ are Dirac indices with values of zero or one; $\delta_{i,j}^{d} = 1$ if the individual died (and zero otherwise), $\delta_{i,j}^{t} = 1$ if the individual was transferred (and zero otherwise), and $\delta_{i,j}^{gs} = 1$ if the individual egg came from a non-distal gall segment (and zero otherwise). Note that, for given i, j, at most one δ can be nonzero. Parameters for a life stage were determined by computationally minimizing *NLL* using the function fminsearch in MATLAB (Mathworks, Inc.), which implements the Nelder-Mead Simplex Method.

Appendix B

B.1 Fitting oviposition and adult lifestage development

To estimate times of oviposition and adult development, we used total time from infestation to emergence at constant 25 °C coupled with observed and censored data for the egg through pupal stages (Section 2.3). First, we fit an overall development curve for the egg through pupal lifestages, which is reasonable because the rate curves for egg, larval instars 1–3, and pupal stages have very similar thresholds and optimum temperatures. This proceeded as with curves for individual life stages, described in Appendix A. There were 108 individuals with complete development at temperatures between 15° C and 34° C, all of which came from eggs in the first gallery segment and therefore required no censoring. The remaining 332 individuals either came from non-terminal gallery segments as eggs, died before pupating, or both. These were all treated as censored observations (i.e., development from egg to pupa must have taken longer than the observed interval).

Because the egg through pupa data, estimated and censored, was essentially fit to intervals of possible emergence, a direct R^2 to measure quality of the fit could not be calculated. Instead, we calculated the pseudo- R^2 of McFadden (Hardin and Hilbe, 2007),

$$R_{McF}^{2} = 1 - \frac{NLL_M}{NLL_0} \tag{B.1}$$

Here NLL_M and NLL_0 refer to the negative log likelihood for the model and a suitable null model, respectively. For a simple null model, we used the empirical summer generations model based on cumulative hours above a threshold of 13 °C (see Results 3.3.1), calculating a mean of 17.47 days required from the 108 individuals that completed development.

Next, we fitted the observed cumulative emergence at 25° C to a log-normal variance model, with a single rate reflecting total rate of development in the population at that temperature and a variance parameter capturing total accumulation of developmental variance across individuals and life phases. To calculate the log-normal fit to timing of total emergence, data on observed emergence/day had to be converted into a list of observed days, with each day replicated in the list according to the number of beetles observed emerging that day. Then mean and variance could be computed on a logarithmic scale,

$$\mu_{25} = \frac{1}{N}\sum_{i,j}\log\left(D_{i,j}\right) \text{ and } \sigma_{25}^{2} = \frac{1}{N-1}\sum_{i,j}\left(\log\left(D_{i,j}\right) - \mu_{25}\right)^2. \tag{B.2}$$

Here $D_{i,j}$ is the day the i th beetle emerged from the j th replicate bolt, with $N = 450$ being the total number of pinyon ips emerging. The predicted distribution of emergence times is then

$$P_{25}(t) = \exp\left[-\frac{\left(\log(t) - \mu_{25} + \frac{1}{2}\sigma_{25}^{2}\right)^2}{2\sigma_{25}^{2}}\right] \Big/ \sqrt{2\pi\sigma_{25}^{2}t^2} \tag{B.3}$$

Note that the additional $\frac{1}{2}\sigma_{25}^{2}$ term in the exponent corrects the mean backwards in time, so that the mean of the log-normal agrees with the observed sample mean (Mangel and Hilborn, 2013).

We then subtracted predicted development from egg to pupa at 25° C from the fitted log-normal description of observed emergence from the four replicate bolts, similar to methods used to estimate adult development rates for mountain pine beetle (Wangen et al., 2024). This gives a predicted distribution of developmental times for the combined ovipositional and adult life phases. To predict a distribution of times for combined oviposition

and adult development we looked for the difference in times between the cumulative density function (CDF) of egg-pupal development and the fitted log-normal CDF for observed total emergence. At a discretization of hourly time steps (i.e., 1/24 day), quantiles of the CDF for total development time were created by direct numerical integration. For each quantile between 0.1 % and 99.9 %, the emergence date for the corresponding egg-pupa developmental quantile was calculated using linear interpolation between the closest two numerical quantiles on the egg-pupa cumulant curve. The difference between the two curves at this quantile is one sample of the developmental difference between egg-pupa development time and total emergence time, which we take to be equivalent to a sample of oviposition plus adult development times.

Next, we fitted this predicted distribution to a log-normal, with a shift in the mean related to mean time for oviposition and adult development (combined) and a variance parameter to predict how developmental variability accrues through these stages. The inferred rate parameter can then be used to rescale the egg-pupa developmental curve by a factor, f_a, and thus calibrate a net development curve for duration of oviposition and maturation of adult Ips. For validation, we compared cumulative emergence from the f_a-scaled egg-pupa model, with estimated variance parameter σ_a^2, and observed emergence from the four replicate bolts at 25 °C.

Next, we estimated the fraction of total oviposition/adult development specifically ascribed to oviposition. The joint oviposition/adult development curve was parsed to reflect oviposition and adult development separately, with an undetermined fraction, f_O, devoted to oviposition (and therefore 1- f_O to adult development). Additionally, because model comparison with Lobo Canyon 2022 emergence cage data suggests there may regional and/or host differences in overall developmental timing (i.e., Utah-sourced beetles from *P. monophylla* compared to New Mexico-sourced beetles from *P. edulis*), we also included a scaling parameter, S_A, to adjust overall development time in the adult and ovipositional stages. Mathematically, this amounts to replacing ψ in the modified Logan curve (Eq. (1)) with $S_A\psi/f_O$ in the ovipositional stage and $S_A\psi/(1-f_O)$ in the adult stage.

Appendix C

C.1 Mechanistic phenology model fitting results

Parameter estimates for the egg through pupal development times based on phloem sandwiches kept at constant temperatures, fitted to a modified Logan rate curve, are provided in Table C.1 (Fig. C.1). The same data were also collectively fitted to the modified Logan rate curve (Table C1; Fig. C.2). The combined egg through pupa fit gave an $R^2_{McF} = 0.7537$ reflecting the relatively poor leverage some of the censored data had on the estimated development curve. Calculating an R^2 using only the median of possible windows of emergence, and only for those individuals which completed and came from eggs 0–1 cm from the distal end of a gallery, gives $R^2 = 0.946$.

The log-normal model for the interval from oviposition to brood adult emergence at constant 25° C suggests a suitable model fit (Fig. C.3). Subtracting combined egg-pupa from the total time yields a distribution of developmental times for the combined ovipositional and adult life phases (Fig. C.4). The calculated mean emergence time for predicted oviposition through adult development is 17.45 days at 25° C, with a standard deviation (on log scales) of $\sigma_a = 0.3201$. The mean development rate for aggregated oviposition and adult development is then $r_a = \frac{1}{16.98} = 0.0589$ day^{-1}. By contrast, the rate of development in the egg through pupal development curve at 25° C is 0.0593 day^{-1}. Thus, we scaled development rates from the egg through pupa development curve to the predicted oviposition to adult curve using the ratio of these rates, $f_a = .0589/.0593 = 0.9932$. Similarly, we scaled the egg through pupa curve to reflect total development (Fig. C.5).

We performed a 'giggle test' by using the egg-pupa model at 25° C and then using the projected development due to ovipositional and adult stages (i.e., scaling down egg-pupal rates by the factor f_a and applying a log-normal cohort model with variance parameter σ_a^2), comparing results against total observed emergence from the four replicate bolts. The giggle test shows a slight discrepancy as cumulative emergence begins to take off, with observed emergence about two days behind predicted emergence (Fig. C.6). This is expected because there is a distribution of eggs oviposited but the model is calibrated as though a single clutch of eggs was oviposited the moment males and females were introduced into the bolts.

The best-fit fraction of total oviposition/adult development specifically ascribed to oviposition, f_O, was estimated as 0.6122. The best-fit scaling parameter, S_A (adjusting joint oviposition/adult development rates from the Utah population to the New Mexico population), was estimated as 1.1205. This is concordant with above Results in that we found evidence that Utah-sourced beetles (reared in *P. monophylla*) have somewhat faster egg-pupa developmental rates than New Mexico-sourced beetles (reared in *P. edulis*).

For comparison with observed field data, the resulting model fit was satisfying compared to observed emergence using observed dates of first attacks and actual phloem temperatures as measured for Lobo Canyon 2022 on two trees (Fig. C.7).

Table C.1
Lifestage-specific and combined egg through pupa parameter estimates for pinyon ips reared in phloem sandwiches at constant temperatures including censored observations fit to a modified Logan rate curve (Hansen et al., 2011). T_m is the upper development threshold and T_b adjusts the location of the lower threshold but is not equal to the lower threshold, which must be determined computationally. The log-normal variance parameter is given by σ; all other parameters are shape parameters.

Lifestage	Egg	L1	L2	L3	Pupa	Egg-pupa
T_b	−12.72041	−1.89944	−2.45593	−1.71550	−0.52761	−1.3972
ψ	0.08656	0.06724	0.02946	0.00533	0.04465	0.01868
ω	0.14425	0.17486	0.18221	0.14967	0.16228	0.13356
Δ_m	6.85157	5.46613	5.19185	3.71990	5.75383	6.9991
T_m	38.84590	36.98041	37.34842	36.26369	37.95438	38.554
σ	0.29671	0.36202	0.28791	0.25150	0.14358	0.13247

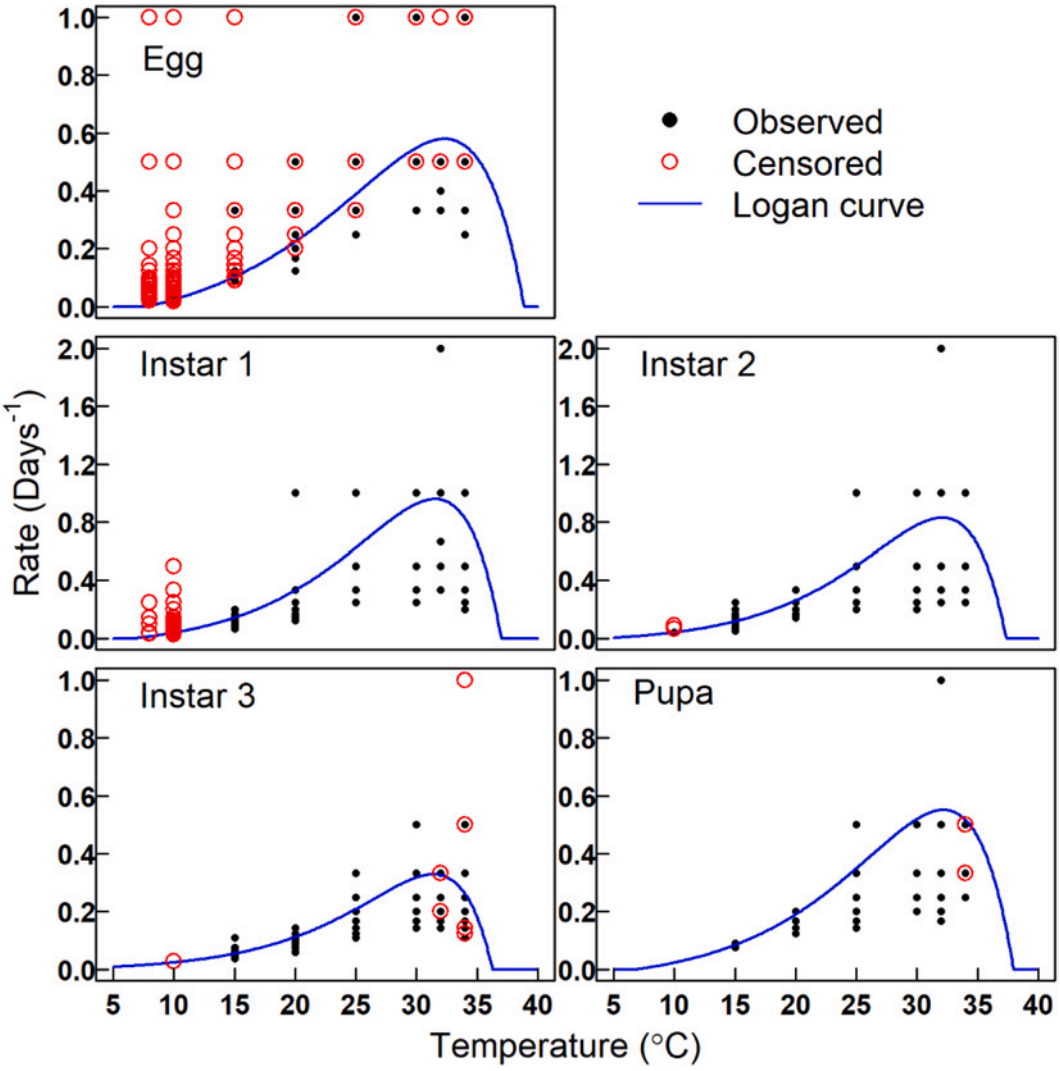

Fig. C.1. Development rate (days^{-1}) of pinyon ips lifestages at a range of constant temperatures, and fitted curves based on the modified Logan model (Hansen et al., 2011). Censored observations in the data occur when the end or beginning of the life-stage was unobserved.

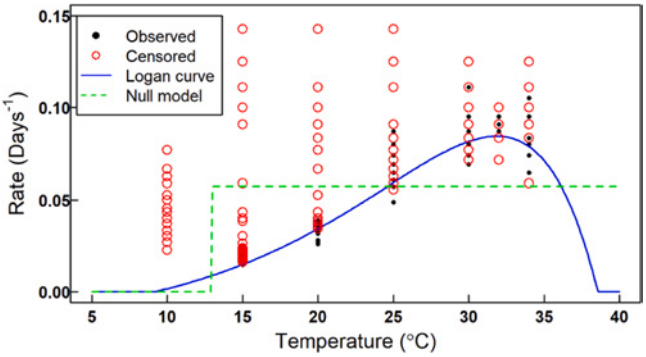

Fig. C.2. Observed (black dots) and censored data (red circles) with fitted Logan rate curve for combined pinyon ips egg through pupa. See Methods for more information.

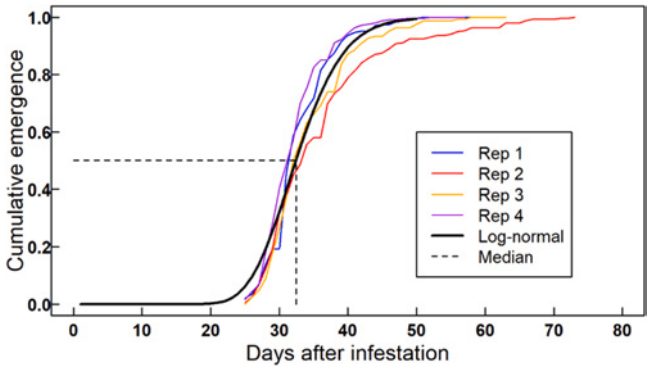

Fig. C.3. Observed pinyon ips emergence from four replicate bolts and log-normal fit. Median emergence occurred on day 32; the mean date of emergence was slightly later, at 33.85 days.

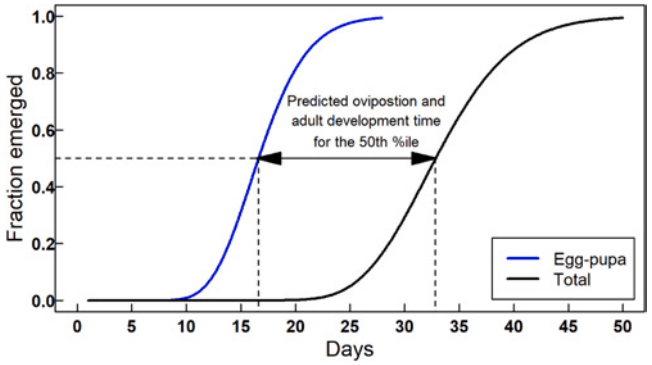

Fig. C.4. Combined pinyon ips oviposition and adult development, at constant 25° C, was estimated by subtracting the combined egg-pupa time from total life cycle time.

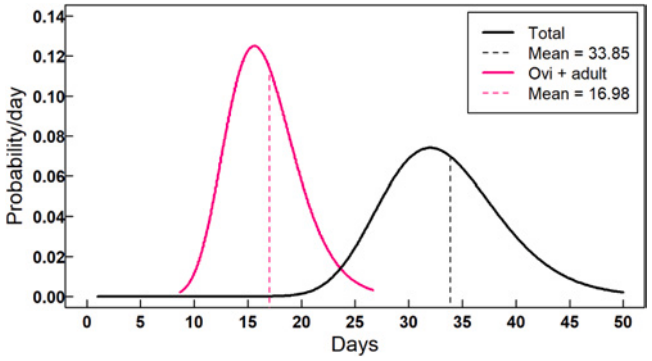

Fig. C.5. Distributions and means of combined pinyon ips oviposition-adult development times compared to the total life cycle.

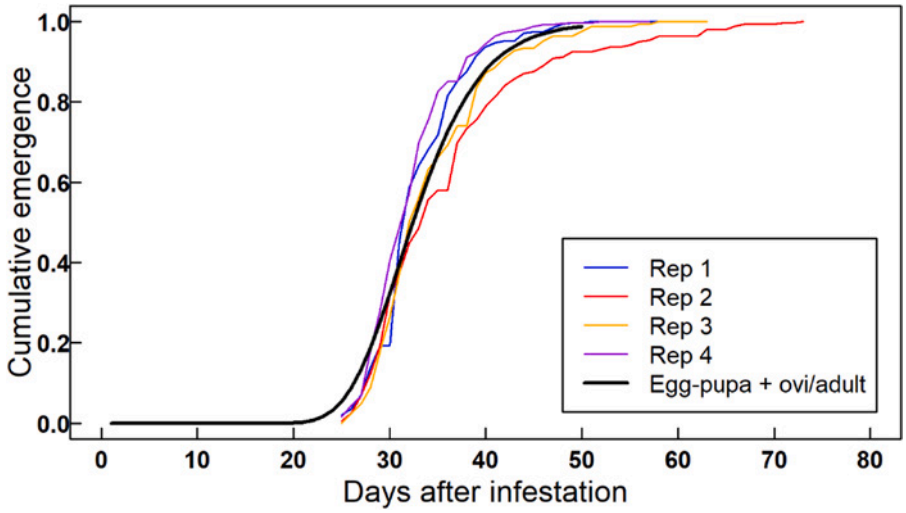

Fig. C.6. Giggle test comparing combined egg through pupa life stages and oviposition and adult development models to observed total life cycle times from infestation to emergence for a pinyon ips population reared at constant 25° C.

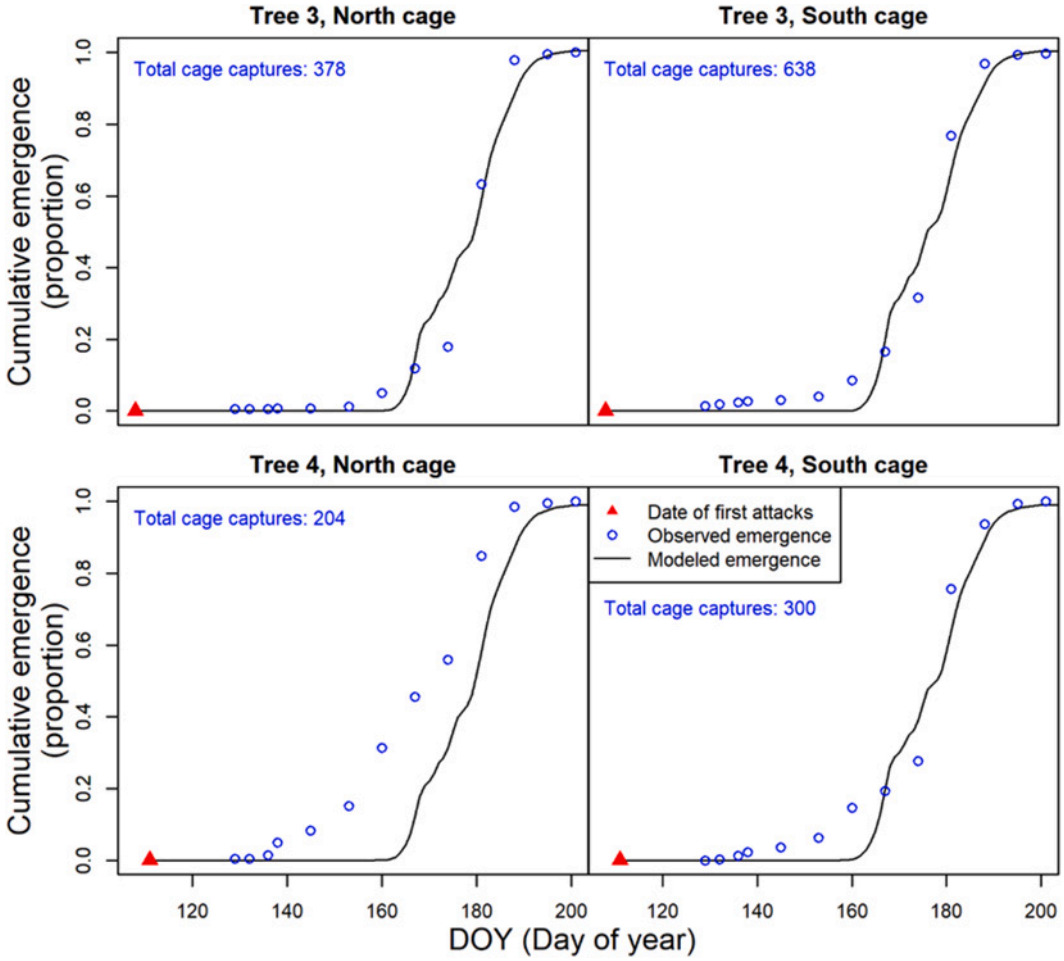

Fig. C.7. Comparison of pinyon ips phenology model predicted (continuous curves) and observed cumulative emergence (discrete markers) on two aspects of two trees in Lobo Canyon with 39 % of overall oviposition/adult development attributed to adult development ($f_O = 0.6122$) and overall development in these stages accelerated by a factor $S_A = 1.1205$. Fitting was achieved by minimizing sum square ***horizontal*** differences (in time) between predictions and observations. Model input was observed phloem temperatures from thermistors placed under each cage, starting with observed dates of first attacks.

Data availability

Data will be made available on request.

References

Baier, P., Pennerstorfer, J., Schopf, A., 2007. PHENIPS—A comprehensive phenology model of *Ips typographus* (L.)(Col., Scolytinae) as a tool for hazard rating of bark beetle infestation. For. Ecol. Manage 249 (3), 171–186.

Barger, R.L., Ffolliott, P.F., 1972. Physical Characteristics and Utilization of Major Woodland Tree Species in Arizona (Vol. 83). Rocky Mountain Forest and Range Experiment Station, Forest Service, US Department of Agriculture.

Bentz, B.J., Logan, J.A., Amman, G.D., 1991. Temperature-dependent development of the mountain pine beetle (Coleoptera: scolytidae) and simulation of its phenology. Can. Entomol 123 (5), 1083–1094. https://doi.org/10.4039/Ent1231083-5.

Bentz, B.J., 2006. Mountain pine beetle population sampling: inferences from Lindgren pheromone traps and tree emergence cages. Can. J. For. Res. 36 (2), 351–360. https://doi.org/10.1139/x05-241.

Bentz, B.J., Cluck, D.R., Bulaon, B.M., Smith, S.L., 2023. Western pine beetle voltinism in a changing California climate. Agric. For. Entomol 25 (4), 637–649. https://doi.org/10.1111/afe.12586.

Birch, M.C., Tilden, P.E., Wood, D.L., Browne, L.E., Young, J.C., Silverstein, R.M., 1977. Biological activity of compounds isolated from air condensates and frass of the bark beetle, *Ips confusus*. J. Insect Physiol 23 (11–12), 1373–1376. https://doi.org/10.1016/0022-1910(77)90160-3.

Bjørnstad, O.N., Nelson, W.A., Tobin, P.C., 2016. Developmental synchrony in multivoltine insects: generation separation versus smearing. Popul Ecol 58, 479–491.

Candau, J.N., Studens, K., 2025. Animal life cycle models (Poikilotherms). In: Schwartz, M.D. (Ed.), Phenology: An integrative Environmental Science. Springer Nature Switzerland, Cham, pp. 339–368.

Chansler, J.F., 1964. Overwintering Habits of *Ips lecontei* Sw. and *Ips confusus* (Lec.) in Arizona and New Mexico (Vol. 27). Rocky Mountain Forest and Range Experiment Station, Forest Service, US Department of Agriculture.

Cibrián-Tovar, D., Méndez Montiel, J.T., Campos Bolaños, R., Yates III, H.O., Flores Lara, J.E., 1995. Forest Insects of Mexico. Chapingo, México: universidad Autonoma Chapingo. Subsecretaria Forestal y de Fauna Silvestre De La Secretaria de Agricultura y Recursos Hidraulicos, México. United States Department of Agriculture, Forest Service, USA. Natural Resources Canada, Canada. North American Forestry Commission, FAO, Publication, 6.

Coulson, R.N., Fargo, W.S., Pulley, P.E., Foltz, J.L., Pope, D.N., Richerson, J.V., Payne, T. L., 1978. Evaluation of the re-emergence process of parent adult Dendroctonus frontalis (Coleoptera: scolytidae). Can. Entomol 110 (5), 475–486.

Crowley, P.H., Hopper, K.R., 2015. Mechanisms for adaptive cohort splitting. Ecol. Model. 308, 1–13.

DeGomez, T., Fettig, C.J., McMillin, J.D., Anhold, J.A., Hayes, C.J., 2014. Managing Slash to Minimize Colonization of Residual Leave Trees By *Ips* and Other Bark Beetle Species Following Thinning in Southwestern Ponderosa Pine. University of Arizona, College of Agriculture and Life Sciences Bulletin, Tucson, AZ, p. 12. AZ1448.

DeLeon, D., Bedard, W.D., Terrell, T.T., 1934. Recent discoveries concerning the biology of the mountain pine beetle and their effect on control in western white pine stands. J. For. 32 (4), 430–436.

Eager, T.J., 1999. Factors affecting the health of pinyon pine trees (*Pinus edulis*) in the pinyon-juniper woodlands of western Colorado. In: Monsen, S.B., Stevens, R. (Eds.), Proceedings: Ecology and Management of Pinyon-Juniper Communities Within the Interior West; 1997 September 15-18; Provo, UT. Proc. RMRS-P-9. U.S. Department of Agriculture, Forest Service, Rocky Mountain Research Station, Ogden, UT, pp. 397–399.

Elzhov, T.V., Mullen, K.M., Spiess, A.-N., Bolker, B., Mullen, M.K.M., 2016. Package 'minpack.Lm.' R interface Levenberg-Marquardt nonlinear least-squares algorithm found in MINPACK plus support bounds. https://cran.r-project.org/web/packages/minpack.lm/minpack.lm.pdf.

Floyd, M.L., Clifford, M., Cobb, N.S., Hanna, D., Delph, R., Ford, P., Turner, D., 2009. Relationship of stand characteristics to drought-induced mortality in three southwestern piñon–juniper woodlands. Ecol. Appl. 19 (5), 1223–1230. https://doi.org/10.1890/08-1265.1.

Gaylord, M.L., Kolb, T.E., McDowell, N.G., 2015. Mechanisms of piñon pine mortality after severe drought: a retrospective study of mature trees. Tree Physiol 35, 806–816. https://doi.org/10.1093/treephys/tpv038.

Gaylord, M.L., Kolb, T.E., Pockman, W.T., Plaut, J.A., Yepez, E.A., Macalady, A.K., et al., 2013. Drought predisposes piñon–juniper woodlands to insect attacks and mortality. New Phytol. 198 (2), 567–578. https://doi.org/10.1111/nph.12174.

Greenwood, D.L., Weisberg, P.J., 2008. Density-dependent tree mortality in pinyon–juniper woodlands. For. Ecol. Manage 255, 2129–2137. https://doi.org/10.1016/j.foreco.2007.12.048.

Hansen, E.M., Bentz, B.J., Turner, D.L., 2001. Physiological basis for flexible voltinism in the spruce beetle (Coleoptera: scolytidae). Can. Entomol 133 (6), 805–817. https://doi.org/10.4039/Ent133805-6.

Hansen, E.M., Bentz, B.J., Powell, J.A., Gray, D.R., Vandygriff, J.C., 2011. Prepupal diapause and instar IV developmental rates of the spruce beetle, *Dendroctonus rufipennis* (Coleoptera: curculionidae, Scolytinae). J. Insect Physiol 57 (10), 1347–1357. https://doi.org/10.1016/j.jinsphys.2011.06.011.

Hansen, E.M., Bentz, B.J., Baggett, L.S., 2024. Evidence for an adult summer diapause in mountain pine beetle (Coleoptera: curculionidae) that varies geographically and among haplogroups. Env. Entomol 53 (5), 837–848. https://doi.org/10.1093/ee/nvae068.

Hardin, J.W., Hilbe, J.M., 2007. Generalized Linear Models and Extensions. Stata Press, p. 387.

Harlow, W.M., Harrar, E.S., White, F.M., 1981. Textbook of dendrology, covering the important forest trees of the United States and Canada. 527 p.

Jakeman, A.J., Elsawah, S., Wang, H.H., Hamilton, S.H., Melsen, L., Grimm, V., 2024. Towards normalizing good practice across the whole modelingcycle: its instrumentation and future research topics. Socio-Environ. Syst. Model. 6, 18755. https://doi.org/10.18174/sesmo.1875.

Kleinman, S.J., DeGomez, T.E., Snider, G.B., Williams, K.E., 2012. Large-scale pinyon ips (*Ips confusus*) outbreak in southwestern United States tied with elevation and land cover. J. For. 110 (4), 194–200. https://doi.org/10.5849/jof.11-060.

Littell, R.C., Milliken, G.A., Stroup, W.W., Wolfinger, R.D., Schabenberger, O., 2006. SAS System for Mixed Models, 2nd ed. SAS Institute, Inc, Cary, North Carolina, United States.

Little Jr., E.L., 1971. Atlas of the United States trees. Volume 1. Conifers and Important hardwoods. Misc. Publ. 1146. U.S. Department of Agriculture, Forest Service, Washington, DC, p. 320.

Lukic, I., Bedoya, C.L., Hofstetter, E.M., Hofstetter, R.W., 2021. Pinyon engraver beetle acoustics: stridulation apparatus, sound production and behavioral response to vibroacoustic treatments in logs. Insects 12, 496. https://doi.org/10.3390/insects12060496.

McManis, A.E., Powell, J.A., Bentz, B.J., 2018. Developmental parameters of a southern mountain pine beetle (Coleoptera: curculionidae) population reveal potential source of latitudinal differences in generation time. Can. Entomol 151 (1), 1–15. https://doi.org/10.4039/tce.2018.51.

Hilborn, R., Mangel, M., 2013. The Ecological detective: Confronting Models With Data (MPB-28). Princeton University Press. *Project MUSE*. https://muse.jhu.edu/book/33194.

Kolb, T.E., Fettig, C.J., Ayres, M.P., Bentz, B.J., Hicke, J.A., Mathiasen, R., Stewart, J.E., Weed, A.S., 2016. Observed and anticipated impacts of drought on forest insects and diseases in the United States. For. Ecol. Manage 380, 321–334.

Meddens, A.J.H., Hicke, J.A., Macalady, A.K., Buotte, P.C., Cowles, T.R., Allen, C.D., 2015. Patterns and causes of observed piñon pine mortality in the southwestern United States. New Phytol. 206, 91–97. https://doi.org/10.1111/nph.13193.

Negrón, J.F., Wilson, J.L., 2003. Attributes associated with probability of infestation by the piñon ips, *Ips confusus* (Coleoptera: scolytidae), in piñon pine, *Pinus edulis*. West. N. Am. Nat. 63, 440–451.

Ogle, K., Whitham, T.G., Cobb, N.S., 2000. Tree-ring variation in pinyon predicts likelihood of death following severe drought. Ecology 81, 3237–3243. https://doi.org/10.1890/0012-9658(2000)081[3237:TRVIPP]2.0.CO;2.

Ostmark, H.E., 1966. The Life history, habits, and Control of the Arizona five-Spined ips, *Ips lecontei* Swaine (Coleoptera: Scolytidae). Univ. of Florida, Gainesville, Florida, p. 79. Ph.D. Dissertation.

Pirtskhalava-Karpova, N., Trubin, A., Karpov, A., Jakuš, R., 2024. Drought initialised bark beetle outbreak in Central Europe: Meteorological factors and infestation dynamic. For. Ecol. Manag. 554, 121666.

Potterf, M., Frühbrodt, T., Thom, D., Lemme, H., Hahn, A., Seidl, R., 2025. Hotter drought increases population levels and accelerates phenology of the European spruce bark beetle *Ips typographus*. For. Ecol. Manage 585, 122615.

Powell, J.A., Bentz, B.J., 2009. Connecting phenological predictions with population growth rates for mountain pine beetle, an outbreak insect. Landsc Ecol 24, 657–672.

R Core Team, 2022. R: a Language and Environment For Statistical Computing. R Foundation for Statistical Computing, Vienna, Austria. URL. https://www.R-project.org/.

Raffa, K.E., Aukema, B.H., Bentz, B.J., Carroll, A.L., Hicke, J.A., Turner, M.G., Romme, W.H., 2008. Cross-scale drivers of natural disturbances prone to anthropogenic amplification: the dynamics of bark beetle eruptions. BioScience 58 (6), 501–517. https://doi.org/10.1641/B580607.

Régnière, J., Powell, J., Bentz, B., Nealis, V., 2012. Effects of temperature on development, survival and reproduction of insects: experimental design, data analysis and modeling. J. Insect Physiol 58 (5), 634–647. https://doi.org/10.1016/j.jinsphys.2012.01.010.

Régnière, J., Powell, J.A., 2013. Animal life cycle models (Poikilotherms). In: Schwartz, M.D. (Ed.), Phenology: An integrative Environmental Science. Dordrecht: Springer, Netherlands, pp. 295–316.

Robbins, Z.J., Xu, C., Aukema, B.H., Buotte, P.C., Chitra-Tarak, R., Fettig, C.J., Goulden, M.L., Goodsman, D.W., Hall, A.D., Koven, C.D., Kueppers, L.M., 2022. Warming increased bark beetle-induced tree mortality by 30% during an extreme drought in California. Glob Chang Biol 28 (2), 509–523.

Santos, M.J., Whitham, T.G., 2010. Predictors of *Ips confusus* outbreaks during a record drought in southwestern USA: implications for monitoring and management. Env. Manage 45, 239–249. https://doi.org/10.1007/s00267-009-9413-6.

Seybold, S.J., Titze, J., Gries, R., Francke, W., 2004. Studies on the aggregation pheromone of the pinyon ips, *Ips confusus* (Coleoptera: scolytidae) in the southwestern United States. Chemical ecology and phytochemistry in forest ecosystems. In: Joint Meeting International Society of Chemical Ecology, 20th annual meeting Phytochemical Society of North America, 39th annual meeting. Canada. University of Ottawa. July 24 to 28, 2004.

Shaw, J.D., Steed, B.E., DeBlander, L.T., 2005. Forest inventory and analysis (FIA) annual inventory answers the question: what is happening to pinyon-juniper woodlands? J. For. 103 (6), 280–285. https://doi.org/10.1093/jof/103.6.280.

Tran, A., Mangeas, M., Demarchi, M., Roux, E., Degenne, P., Haramboure, M., et al., 2020. Complementarity of empirical and process-based approaches to modelling mosquito population dynamics with Aedes albopictus as an example—Application to the development of an operational mapping tool of vector populations. PloS one 15 (1), e0227407.

USDA Forest Service, 2025. Forest insect and disease conditions in the Southwestern Region. https://www.fs.usda.gov/r03/natural-resources/forest-health.

Wagner, T.L., Gagne, J.A., Sharpe, P.J., Coulson, R.N., 1984. A biophysical model of southern pine beetle, *Dendroctonus frontalis* Zimmermann (Coleoptera: scolytidae), development. Ecol Modell 21, 125–147.

Wangen, C.E., Powell, J.A., Bentz, B.J., 2024. A mountain pine beetle (Coleoptera: curculionidae) adult development rate model confirms evolved geographic differences. J. Insect Sci. 24 (4), 16. https://doi.org/10.1093/jisesa/ieae074.

Webb, M., 1999. Importance of pinyon-juniper habitat to birds. In: Proceedings: Ecology and Management of Pinyon-Juniper Communities Within the Interior West. Rocky Mountain Research Station, pp. 15–18. RMRS-P-9.

Wermelinger, B., Seifert, M., 1998. Analysis of the temperature dependent development of the spruce bark beetle *Ips typographus* (L) (Col., Scolytidae). J. Appl. Entomol. 122, 185–191.

Wilkinson, R.C., 1963. Larval instars and head capsule morphology in three southeastern *Ips* bark beetles. Fla. Entomol 46, 19–22.

Wood, S.L., 1982. The bark and ambrosia beetles of North and Central America (Coleoptera: scolytidae), a taxonomic monograph. Gt. Basin Nat. Mem. 6, 1–1359.